JAMES | Journal of Advances in Modeling Earth Systems

RESEARCH ARTICLE
10.1029/2021MS002842

The Madden–Julian Oscillation in the Energy Exascale Earth System Model Version 1

Daehyun Kim[1], Daehyun Kang[2], Min-Seop Ahn[3], Charlotte DeMott[4], Chia-Wei Hsu[4], Changhyun Yoo[5], L. Ruby Leung[6], Samson Hagos[6], and Philip J. Rasch[6]

[1]Department of Atmospheric Sciences, University of Washington, Seattle, WA, USA, [2]Department of Oceanography, Chonnam National University, Gwangju, South Korea, [3]PCMDI, Lawrence Livermore National Laboratory, Livermore, CA, USA, [4]Department of Atmospheric Science, Colorado State University, Fort Collins, CO, USA, [5]Department of Climate and Energy Systems Engineering, Ewha Womans University, Seoul, South Korea, [6]Pacific Northwest National Laboratory, Richland, WA, USA

Key Points:

- Energy Exascale Earth System Model version 1 (E3SMv1) simulates Madden-Julian Oscillation (MJOs) that exhibit realistic eastward propagation over the Indo-Pacific warm pool
- Modeled processes of the MJO, revealed through column-integrated moist static energy anomalies, match well with those in observations
- Despite the decent MJO simulation fidelity, the observed MJO–Quasi-Biennial Oscillation coupling is not simulated in E3SMv1

Correspondence to:
D. Kim and D. Kang,
daehyun@uw.edu;
dhkang223@gmail.com

Citation:
Kim, D., Kang, D., Ahn, M.-S., DeMott, C., Hsu, C.-W., Yoo, C., et al. (2022). The Madden–Julian oscillation in the energy Exascale Earth System Model version 1. *Journal of Advances in Modeling Earth Systems*, *14*, e2021MS002842. https://doi.org/10.1029/2021MS002842

Received 23 SEP 2021
Accepted 7 JAN 2022

Abstract The present study examines the characteristics of the Madden–Julian Oscillation (MJO) events represented in the Energy Exascale Earth System Model version 1 (E3SMv1), DOE's new Earth system model. The coupled E3SMv1 realistically simulates the eastward propagation of precipitation and moist static energy (MSE) anomalies associated with the MJO. As in observations, horizontal moisture advection and longwave radiative feedback are found to be the dominant processes in E3SMv1 that lead to the eastward movement and maintenance of the MJO MSE anomalies, respectively. Modulation of the diurnal cycle of precipitation in the Maritime Continent region by the MJO is also well represented in the model despite systematic biases in the magnitude and phase of the precipitation diurnal cycle. On the MJO impact over the midlatitude, E3SMv1 reasonably captures the pattern of the MJO teleconnections across the North Pacific and North America, with improvement in the performance in a high-resolution version, despite the magnitude being a bit weaker than the observed. Regarding the interannual variability of the MJO, the El Niño-Southern Oscillation (ENSO) modulation of the zonal extent of MJO's eastward propagation, as well as associated changes in the mean state moisture gradient in the tropical west Pacific, are well reproduced in the model. However, MJO in E3SMv1 exhibits no sensitivity to the Quasi-Biennial Oscillation (QBO), with the MJO propagation characteristics being almost identical between easterly QBO and westerly QBO years. Processes that have been suggested as critical to MJO simulation are also examined by utilizing recently developed process-oriented diagnostics.

Plain Language Summary The United States Department of Energy developed a new computer model that simulates Earth's climate systems, called Energy Exascale Earth System Model version 1 (E3SMv1). This study examines how well the model reproduces the characteristics of the Madden–Julian Oscillation (MJO), a tropical climate phenomenon that impacts weather and climate around the globe. We find that the strength and eastward movement of the MJO is realistically represented in the model. Variability of water vapor and radiation are the dominant processes for the MJO simulation, which agree well with the real-world observations. Despite some unrealistic features, E3SMv1 successfully simulates the impact of the MJO on tropical precipitation at shorter than daily time scale and on large-scale atmospheric circulation in the midlatitude. The model also exhibits realistic year-to-year changes in east-west expansion of the MJO by the El Niño-Southern Oscillation, while no noticeable changes can be detected when stratospheric wind reverses its direction over the equator in every 1 or 2 years.

1. Introduction

Extreme weather and climate events, such as landfalling tropical cyclones, cold surges, and droughts, present a significant threat to heavily populated areas and have profound socio-economic impacts on many economic sectors, including energy, agriculture, and water resource management. As the occurrence frequency of extreme events is expected to increase with greenhouse gas-induced global warming, it is challenging to develop mitigation strategies for future extreme events. At the heart of those efforts are short-term predictions and long-term projections of extreme events, whose accuracy and reliability depend strongly on the fidelity of the numerical models used to produce them.

As the dominant source of Earth system predictability at the intraseasonal time scale, the Madden–Julian oscillation (MJO; Madden & Julian, 1971, 1972) is a known driver of many types of extreme events all over the globe (Zhang, 2013). Examples of the extreme events affected by the MJO include extreme rainfall (e.g., Jones & Carvalho, 2012), flooding (e.g., Bond & Vecchi, 2003), cold surges (e.g., Jeong et al., 2005), fire (e.g., Reid et al., 2012), lightning (e.g., Abatzoglou & Brown, 2009), tornado (e.g., Thompson & Roundy, 2013), tropical cyclones (e.g., Klotzbach, 2014), and atmospheric rivers (e.g., Zhou et al., 2021; Hagos, Leung, Garuba, & Patricola, 2021). Given the MJO's bold fingerprint on the location, frequency, and intensity of these extreme events, a realistic representation of the MJO is arguably a prerequisite for any numerical weather and climate models to accurately simulate the societally relevant extreme events.

The main goal of the present study is to examine the characteristics of the MJO and its teleconnections in the Energy Exascale Earth System Model version 1 (E3SMv1; Golaz et al., 2019; Leung et al., 2020), a fully coupled Earth system model developed as part of the ongoing E3SM program (e3sm.org) of the U.S. Department of Energy. Despite recent collective efforts to evaluate the performance of the model (Leung et al., 2020 and references therein), its MJO simulation fidelity has been only briefly documented in Golaz et al. (2019), who showed that the eastward propagation of the MJO is realistically represented in the ocean-atmosphere coupled version of E3SMv1 (their Figure 22), in Caldwell et al. (2019), who briefly compared the MJO in E3SMv1 at low (∼100 km) and high (∼25 km) resolutions, and in Orbe et al. (2020), who compared the MJO among other modes of variability in six U.S. climate models including E3SMv1. Our study provides the first in-depth analysis of the MJO variability in E3SMv1 simulations.

While significant progress has been made in MJO modeling in the past few decades (readers are referred to Kim & Maloney, 2017, and Jiang et al., 2020 for reviews on the history of MJO modeling), an accurate representation of the MJO and its teleconnections is still one of the most challenging tasks for many GCMs (Ahn et al., 2017; Ahn, Kim, Kang, et al., 2020; Jiang et al., 2015; Wang et al., 2020a, 2020b). A particular aspect of MJO variability that most contemporary GCMs struggle with is the poor representation of the MJO interaction with the islands in the Maritime Continent (MC). The MJO exhibits peculiar behaviors when it propagates across the MC region, with its propagation sometimes ceasing (e.g., DeMott et al., 2018; Feng et al., 2015; Kerns & Chen, 2020; Kim, Kug, & Sobel, 2014; Zhang & Ling, 2017) and its convection detouring around the MC islands toward the summer hemisphere (e.g., Kim et al., 2017; Wang & Rui, 1990; Wu & Hsu, 2009). In many GCMs, MJO propagation is disrupted too frequently, suggesting that the 'barrier' effects of MC islands on the MJO are exaggerated (e.g., Ling et al., 2017). While the land-sea contrast (e.g., Sobel et al., 2010), the steep topography (e.g., Wu & Hsu, 2009), the persistent diurnal cycle of precipitation in the MC islands (e.g., Hagos et al., 2016; Zhang & Ling, 2017), and the mean state moisture gradient on the eastern side of Sumatra and Borneo (e.g., Jiang et al., 2019) have all been suggested as key aspects of the MC that damp MJO variability there, the leading mechanisms through which the MC islands affect MJO convection remain elusive. Reviews on this topic can be found in Jiang et al. (2020) and Kim et al. (2021). To our knowledge, no study has systematically examined how well GCMs simulate the southward detouring of the MJO during boreal winter.

Another aspect of MJO variability that is poorly represented in GCMs is the year-to-year variability. While many studies have documented how observed MJO events are affected by the El Niño southern oscillation (ENSO; e.g., Gushchina & Dewitte, 2012; Kang et al., 2021; Pohl & Matthews, 2007; Tam & Lau, 2005; Wei & Ren, 2019; Woolnough et al., 2000; Zhang & Han, 2020) and the quasi-biennial oscillation (QBO; Hendon & Abhik, 2018; Martin, Son, et al., 2021 Nishimoto & Yoden, 2017; Son et al., 2017; Yoo & Son, 2016; Zhang & Zhang, 2018), understanding of the underlying mechanisms of MJO modulation by low-frequency modes remains incomplete. Despite the statistically robust QBO–MJO relationship present in observations, no existing GCM seems to be able to reproduce the observed QBO–MJO relationship (Kim et al., 2020; Lee & Klingaman, 2018), even with a QBO signal given through nudging (Martin, Orbe, et al., 2021). Richter et al. (2019) showed that E3SMv1 simulates a QBO with a periodicity and amplitude that are shorter and larger, respectively, than observed; nonetheless, it is worthwhile to investigate whether and how strongly the QBO modulation of the MJO is simulated in the model.

Careful examination of model simulations can provide useful insights not only into the mechanism of the phenomenon of interest but also into model biases at the process level. Recent efforts to develop process-oriented MJO simulation diagnostics have emphasized moisture-convection coupling (e.g., Kim, Xavier, et al., 2014), the gross moist stability (e.g., Benedict et al., 2014), cloud-radiation feedback (e.g., Kim et al., 2015), and the horizontal gradient of mean moisture (Ahn, Kim, Kang, et al., 2020; DeMott et al., 2019; Gonzalez & Jiang, 2017;

Jiang, 2017; Kang et al., 2020) as the processes that are crucial for a model to be able to generate MJO variability internally. Meanwhile, the moist static energy (MSE) and moisture budget of the MJO in observations/reanalysis products have also been documented in detail (e.g., Kim, Kug, & Sobel, 2014; Kiranmayi & Maloney, 2011; Maloney, 2009; Ren et al., 2021; Sobel et al., 2014). By focusing on phenomena that are directly affected by the parameterization schemes of deep convection, clouds, and radiation, the process-based diagnostics can offer insights as to whether and how the parameterizations need to be improved. These diagnostics can also help assess whether the model simulates the MJO for the correct reason.

In this study, we will analyze simulations made with E3SMv1 to investigate MJO propagation, the MJO MSE budget, MJO teleconnections to the midlatitudes, the interaction of the MJO with the MC islands, and the MJO-ENSO and MJO-QBO relationships. Processes that have been suggested as critical to MJO simulation will be examined by utilizing recently developed process-oriented diagnostics, which can guide further model development.

The manuscript is organized as follows. The model simulations and the reference datasets are described in Section 2. The diagnostics used in the analysis are explained in Section 3. In Section 4, we present the result of performance-based and process-based diagnosis of MJO variability in E3SMv1 simulations, which is followed by a summary and conclusions in Section 5.

2. Model and Data

2.1. Reference Data

In this study, The National Oceanic and Atmospheric Administration (NOAA) daily interpolated Outgoing Longwave Radiation (OLR) product (Liebmann & Smith, 1996) is used as a proxy for tropical convection. The rain rate is taken from the Tropical Rainfall Measuring Mission (TRMM) Multi-satellite Precipitation Analysis (TMPA). The TRMM data set used in this study is the post-real-time data of version 7 (3B42), with a temporal resolution of 3 hr and spatial resolution of $0.25° \times 0.25°$ (Huffman et al., 2007). For sea surface temperature (SST), the Hadley Centre Sea Ice and SST (Rayner et al., 2003) data set is used.

Various atmospheric state variables and the turbulent and radiative fluxes at the lower and upper boundaries of the atmosphere are obtained from the fifth generation of the European Centre for Medium-Range Weather Forecasts (ECMWF) reanalysis (ERA5) product (Hersbach et al., 2020).

The OLR and ERA5 data are obtained for the period 1979–2018, and the TRMM rain rate for 1998–2018. All data are interpolated onto a $2.5°$ longitude $\times$ $2.5°$ latitude horizontal grid. In this study, we primarily focus on boreal winter from November to April (NDJFMA) when the MJO and its teleconnection to the extratropics are most pronounced. As an exception to this, the interannual variability of the MJO is investigated in DJF (Section 4.6).

2.2. E3SM Version 1

E3SMv1 has been developed from the Community Earth System Model version 1 (CESM1) and by including numerous changes in the atmosphere and by replacing ocean, sea ice, and land ice models, all based on the Model for Prediction Across Scales (MPAS) that uses spherical centroidal voronoi tessellations for multiresolution modeling. The E3SMv1 atmosphere model (EAM, Rasch et al., 2019; Xie et al., 2018) is based on the Community Atmosphere Model version 5 (CAM5), but with updates to the cloud microphysics, shallow convection, aerosol, and turbulence parameterizations. The vertical resolution was more than doubled (30–72 levels) and model top raised to allow an improved treatment of the lower stratosphere relative to CAM5. With the release of E3SMv1 in April 2018 both the low-resolution (LR, Golaz et al., 2019) and high-resolution (HR, Caldwell et al., 2019) model versions, where the atmosphere model is applied at a grid spacing of $\sim$100 and $\sim$25 km, respectively, are available. The LR and HR versions of the model use somewhat different parameter settings to optimize model fidelity in the two model configurations, so differences are not due solely to resolution. Readers are referred to Leung et al. (2020) and references therein for the overview of development of E3SM and the evaluation of its performance.

Three sets of coupled simulations made with E3SMv1 are analyzed in this study. The 5-member ensemble Historical (1850–2014) simulation conducted with LR E3SMv1, which is available from the CMIP6 archive, is used

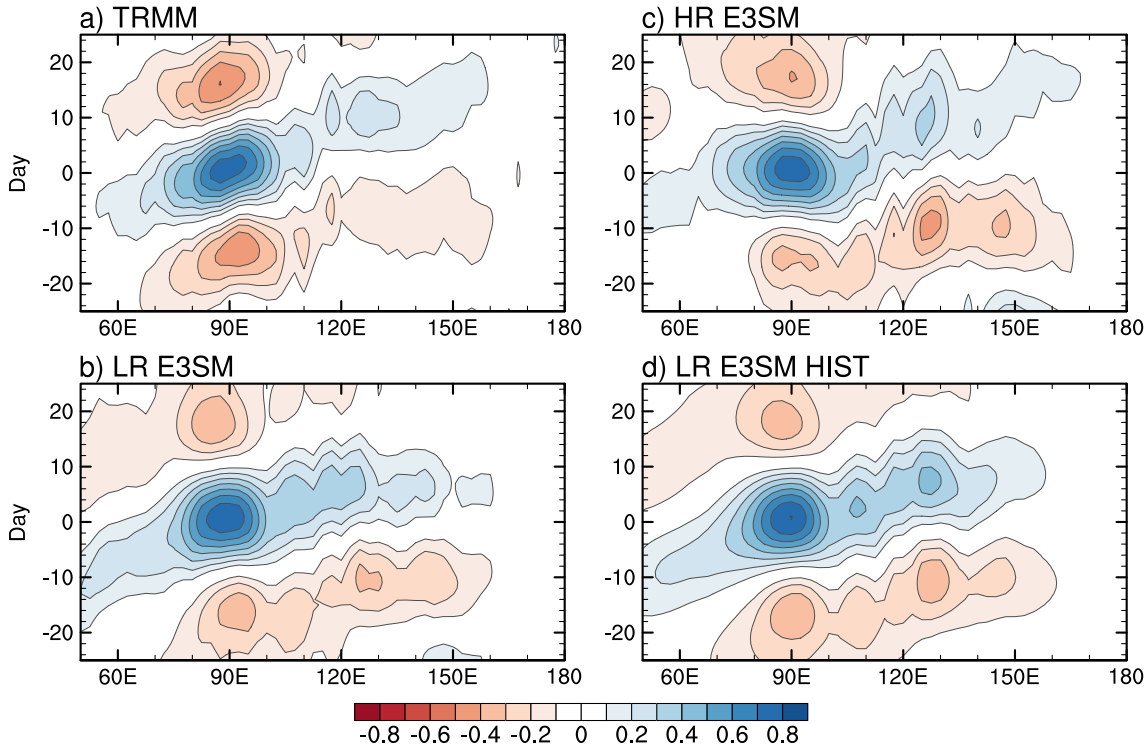

Figure 1. Longitude–lag diagram of equatorial (10°S–10°N) precipitation regressed against intraseasonal precipitation anomalies in the Indian Ocean reference region (5°S–5°N, 85–95°E) during NDJFMA for (a) Tropical Rainfall Measuring Mission and (b–d) Energy Exascale Earth System Model version 1 simulations. For (b) and (c) low resolution and high resolution simulations of a recent 20-year period are used, while for (d) the lag–regression diagram is first obtained from each of the five ensemble members of the CMIP6 Historical simulation (1850–2014) and then averaged across all ensemble members.

to investigate the interannual variability of the MJO (Section 4.6). While covering a long period (165 years) and thereby providing enough samples for the examination of year-to-year variability, not all variables needed for detailed process studies are available from the Historical simulation. By branching off from one ensemble member of the Historical ensemble simulation, we performed a 20-year (1995–2014) simulation with LR E3SMv1 by saving many atmospheric variables and turbulent and radiative fluxes at the surface and the top of the atmosphere at a 6-hourly interval. In addition, a 20-year (1957–1976) simulation (Balaguru et al., 2020) made with HR E3SMv1, as an extension of the 50-year run reported by Caldwell et al. (2019) with time-invariant 1950s forcing, is used. Note that the output from the 20-year simulations made with LR and HR E3SMv1 are our primary data set for most diagnostics. For the MJO MSE budget and MJO process-oriented diagnostics, only LR E3SMv1 is examined.

Figure 1 shows the longitude-lag diagrams of equatorial (10°S–10°N), intraseasonal precipitation anomalies regressed onto the Indian Ocean (5°S–5°N, 85–95°E) reference time series from observations (Figure 1a) and from the three model simulations (Figures 1b–1d). The observed eastward propagation of intraseasonal precipitation anomalies associated with the MJO (Figure 1a) is reasonably reproduced in all E3SMv1 simulations used in this study (Figures 1b–1d). A feature that is worth noting is that the MJO signal in LR E3SMv1 is greater than observed in the MC region (110°–140°E), suggesting the MJO experiences a weaker MC barrier effect in the model than in the observations. Comparison with HR E3SMv1 indicates that employing a higher horizontal resolution did not improve the MJO simulation, consistent with Caldwell et al. (2019) based on comparison of the precipitation power spectra at low and high resolutions. HR E3SMv1 features a somewhat faster and weaker MJO propagation in the MC region (Figure 1c). Lastly, MJO propagation characteristics are qualitatively similar between the 20-year (Figure 1b) and the Historical ensemble simulations (Figure 1d).

3. Diagnosis of MJO and Its Teleconnections

In this section, we provide brief descriptions of the specific diagnostics that are used in this study to examine processes associated with the MJO and MJO teleconnections.

3.1. MJO Life-Cycle Composite

To extract the MJO signal from observations and model simulations, we use a method that is similar to that of Wheeler and Hendon (2004), which is often referred to as the MJO life-cycle composite. For each data set of interest, we obtain the combined empirical orthogonal functions (CEOFs) of 15°S–15°N averaged, intraseasonal (20–100 days bandpass filtered) anomalies of OLR and zonal wind at 850 and 200-hPa. For model simulation data, the resulting two leading CEOFs are rotated to best match the pattern of the observed counterparts. Once the leading pair of CEOFs are obtained, the corresponding PCs are used to define the 'phase' and 'amplitude' of the MJO, following Wheeler and Hendon (2004). The MJO life-cycle composite can be constructed for any atmospheric field or flux variable by averaging intraseasonal anomalies of the variable for each MJO phase (total of 8 "Real-Time Multivariate MJO" (RMM) phases) with an amplitude threshold of 1.

3.2. MJO MSE Budget

To examine the moistening process associated with the maintenance and propagation of the MJO, we use the intraseasonal, vertically integrated MSE budget equation:

$$\left\langle \frac{\partial m}{\partial t} \right\rangle' = \langle \overrightarrow{V} \bullet \nabla_h m \rangle' - \left\langle \omega \frac{\partial m}{\partial p} \right\rangle' + LH' + SH' + \langle LW \rangle' + \langle SW \rangle' + res_m, \tag{1}$$

where m is MSE ($=C_pT + gz + L_vq$), C_p is the specific heat of dry air at constant pressure, g is the gravitational constant, L_v is the latent energy of vapourization, T, q, LH and SH are temperature, specific humidity, surface latent and sensible heat fluxes, respectively, and LW and SW are longwave and shortwave radiative heating rates, respectively. res_m is the budget residual, which is obtained by subtracting all RHS terms from MSE tendency. The prime indicates an intraseasonal anomaly, and the angle brackets denote the mass-weighted vertical integral from the surface to 100 hPa. The MSE budget analysis has been used to examine the propagation and maintenance of the MJO in observations and model simulations (e.g., Andersen & Kuang, 2012; Arnold et al., 2013; Kim, Kug, & Sobel, 2014; Kiranmayi & Maloney, 2011; Maloney, 2009). The relative contribution of the individual MSE budget terms to the maintenance (S_m) and propagation (S_p) of MSE anomalies can be estimated by projecting them upon MSE anomalies and their tendencies (e.g., Andersen & Kuang, 2012):

$$S_m(F) = \frac{||F' \cdot M'||}{||M' \cdot M'||}, \tag{2a}$$

$$S_p(F) = \frac{||F' \cdot \partial M'/\partial t||}{||\partial M'/\partial t \cdot \partial M'/\partial t||}, \tag{2b}$$

where F' and M' are column-integrated MSE budget terms and MSE anomaly, respectively, and ||A|| is the integral of variable A over the domain 60°–180°E, 20°S–10°N, and MJO phases 1–8 in the MJO life-cycle composite.

3.3. MJO Teleconnections

The lagged life-cycle composite is used to analyze the evolution of mid-latitude circulation anomalies associated with the MJO. For example, for MJO phase 3, days with an active (i.e., amplitude >1) MJO are defined as zero lag days, and the lagged composites are constructed by averaging 500-hPa geopotential height anomalies for the successive lag days without an MJO amplitude constraint. To obtain patterns and daily time series of the Pacific North American (PNA) teleconnection, we perform the Rotated Principal Component Analysis with daily 500-hPa geopotential height anomalies in the region between 0°N and 90°N (Barnston & Livezey, 1987; Feldstein, 2000). In observations and E3SMv1, the PNA pattern emerges as the third and first leading modes, respectively (not shown). The PNA index is obtained by projecting the pattern onto the daily anomalies over the North Pacific and North America (0°–90°N, 150°E–30°W).

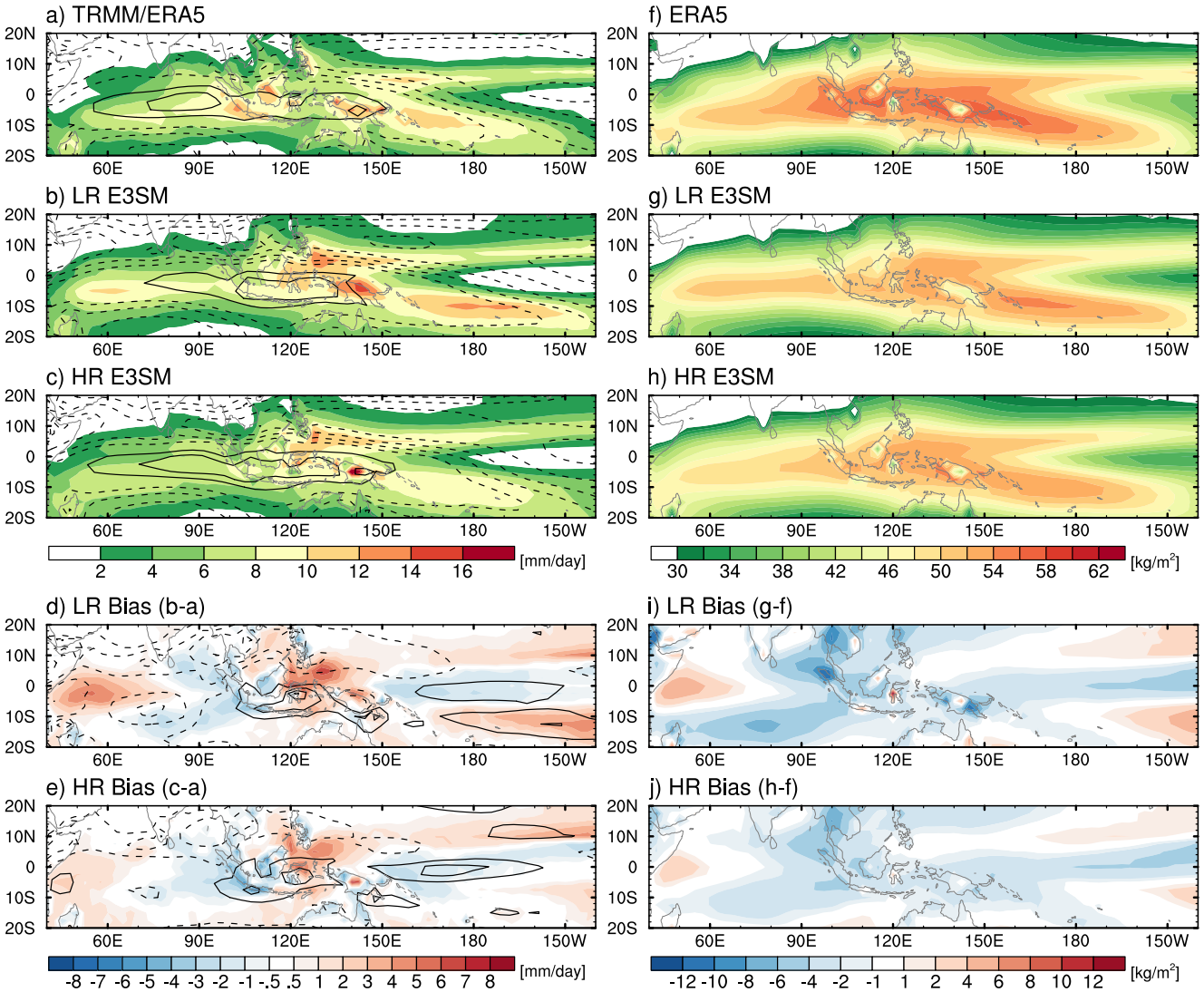

Figure 2. November–April mean state of (a, b, and c) precipitation (mm day^{-1}, shaded) and 850-hPa zonal wind (m s^{-1}, contour), and (f, g, and h) precipitable water (kg m^{-2}, shaded). The top three panels show observations, low resolution Energy Exascale Earth System Model version 1 (LR E3SMv1), and high resolution E3SMv1 (HR E3SMv1), respectively, while the bottom two rows show the biases in LR E3SMv1 and HR E3SMv1, respectively. The contour interval for 850-hPa zonal wind is 2 m s^{-1}. For the bias, the contour intervals are 1 m s^{-1} for 850-hPa zonal wind. In all panels, the zero lines are omitted.

4. Results

4.1. Mean State

From a perspective in which the MJO is defined as fluctuations around the climatological seasonal cycle, it is reasonable to assume that the mean state would have profound impacts on the characteristics of the MJO. In fact, many processes associated with the propagation and maintenance of the MJO have been suggested to be strongly affected by various features of the mean state, such as the zonal extent of the mean westerly wind near the equator over the warm pool (e.g., Inness et al., 2001), gross moist stability (e.g., Benedict et al., 2014), and horizontal gradient of mean moisture (e.g., Ahn, Kim, Kang, et al., 2020; Ahn, Kim, Ham, et al., 2020; DeMott et al., 2019; Gonzalez & Jiang, 2017; Jiang, 2017; Kang et al., 2020). In this subsection, we focus on the mean state over the Indo-Pacific warm pool, which consists of two ocean basins—the Indian Ocean and the western Pacific—and the archipelago in between, where the convective signal associated with the MJO is most active.

Figure 2 shows that the mean precipitation, 850-hPa zonal wind and precipitable water (PW) are reasonably simulated in LR and HR E3SMv1, though there are some systematic biases in each field. In the Indian Ocean and west

Pacific, both versions of E3SMv1 exhibit a positive and a negative precipitation bias on the western and eastern sides of the basins, respectively. As a result, the zonal gradient of the mean precipitation across the Indian Ocean is weaker than observed, while the opposite is the case in the western Pacific. In the tropical Pacific, especially to the east of the dateline, the model exhibits wet biases in the subtropics that are straddling a dry bias near the equator. It is worthwhile to note that this pattern of precipitation bias is common to many CMIP6 models (e.g., Figure 1c in Hagos, Leung, Garuba, Demott, et al., 2021), suggesting that the bias is rooted in a systematic bias in the representation of moist physics (Hagos, Leung, Garuba, Demott, et al., 2021). The mean westerly wind in the equatorial Indian Ocean is underestimated in LR E3SMv1, presumably due to the weaker-than-observed zonal gradient in the mean precipitation. On the contrary, the mean westerly wind is overestimated in the MC(between 100° and 140°E) in LR and HR E3SMv1, with positive and negative precipitation biases prevailing on the eastern and western sides of the region, respectively.

The mean PW bias pattern overall mimics that of the mean precipitation, with a dry bias prevailing in the Indo-Pacific warm pool area in both versions of E3SMv1. It has been shown in Golaz et al. (2019) and Caldwell et al. (2019) that the LR and HR E3SMv1 exhibit a weak warm SST bias in many parts of the Indo-Pacific warm pool, suggesting that the dry bias likely stems from the bias in moist physics. The climatological meridional moisture gradient is steeper in LR E3SMv1 than in ERA5 in the central and eastern Indian Ocean, with the magnitude of the dry bias being larger in the off-equatorial area than near the equator. In contrast, the zonal gradient in the mean PW is underestimated in LR and HR E3SMv1 in the equatorial Indian Ocean. The role of the mean state moisture gradient, especially that of the meridional gradient, on the propagation of the MJO in E3SMv1 will be further discussed in Section 4.3.

4.2. MJO Propagation Characteristics

Figure 3 shows the MJO life-cycle composite (Section 3.1) of precipitation (shaded) and column MSE anomalies (contours) for eight MJO phases. For HR E3SMv1, only precipitation anomalies are shown because the 3-D variables required to calculate MSE are not available. The geographical distribution of MJO precipitation anomalies is reasonably represented in both versions of E3SMv1, although their magnitude is underestimated in HR H3SMv1. In observations, during phase 1, anomalously enhanced convection associated with positive column MSE anomalies is located in the western and central Indian Ocean. Dry conditions prevail over the MC region, except in Borneo and Sumatra islands, where both precipitation and column MSE show near-zero or slightly positive anomalies. LR and HR E3SMv1 successfully capture this 'vanguard' precipitation signal (Peatman et al., 2014) in the MC islands, although its magnitude and the zonal extent to the east are slightly overestimated.

The development of positive precipitation anomalies in the eastern Indian Ocean during MJO phases 2 and 3 in E3SMv1 is not as pronounced as in observations, possibly due to the dry bias in the mean state there (Figure 2). A branch of MJO-related anomalous convection in the equatorial western Pacific appears in phase 3 and matures in phase 4 in the observations. This development of enhanced convection in the western equatorial Pacific and subsequently along the intertropical convergence zone occurs mostly in the northern hemisphere. In LR E3SMv1, the corresponding precipitation anomalies develop earlier than in observations by about 1 MJO phase (~5–8 days), indicating that the stronger-than-observed vanguard effect is related to the early onset of convection in the northern branch.

Another branch of MJO-associated convection anomalies propagates more slowly and mostly to the south of the equator, which has been described as the 'detouring' signal around the MC islands (e.g., Kim et al., 2017; Wang & Rui, 1990). This branch of anomalous convection reaches the western Pacific in phase 6 and matures in phase 7, about 3 phases (~15–24 days) later than its northern counterpart. LR and HR E3SMv1 capture remarkably well the propagation of the southern branch along the oceanic channel between the MC islands and Australia in phases 4 and 5 and the subsequent development of MJO convection along the south Pacific convergence zone in phases 6 and 7.

4.3. MJO MSE Budget

Intraseasonal variability of column MSE is mainly governed by that of column water vapor in the tropics (Wolding et al., 2016). In Figure 3, it is shown that precipitation and column MSE anomalies are positively correlated with each other in observations and in LR E3SMv1, suggesting that useful insights into the propagation and

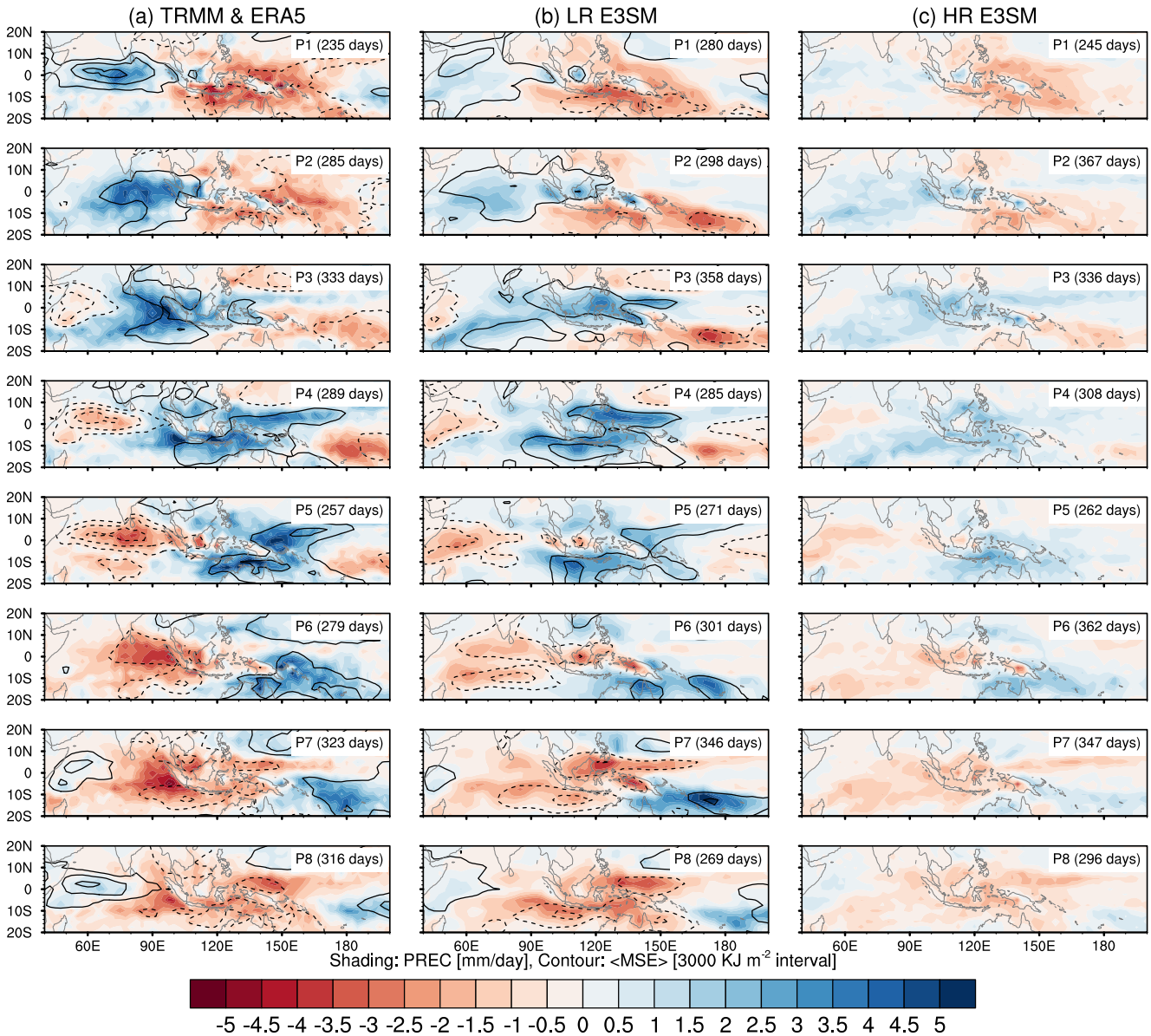

Figure 3. Madden-Julian oscillation (MJO) life cycle composite maps of intraseasonal precipitation (mm day^{-1}, shaded) and column-integrated moist static energy (MSE) anomalies (kJ m^{-2}, contour) obtained from each Real-Time Multivariate MJO (RMM) phase (RMM amplitude >1) during NDJFMA: (a) observations, (b) low resolution Energy Exascale Earth System Model version 1 (E3SMv1), and (c) high resolution E3SMv1. The contour interval for column-integrated MSE anomalies is 3000 kJ m^{-2}. The number of days used in each phase composite is indicated in the parentheses.

maintenance of the MJO precipitation anomalies can be obtained by examining the column MSE budget. Figure 4 shows the MSE budget terms (Equation 1) during MJO phases 2 and 3 in observations (left) and LR E3SMv1 (right), while the relative contribution of each budget term on the propagation and maintenance of MJO MSE anomalies are displayed in Figure 5.

By design, the MSE tendency term is 90° out of phase with MSE anomalies, showing positive (i.e., moistening) and negative (i.e., drying) tendency to the east and west of positive MSE anomalies (first row in Figure 4). In LR E3SMv1, the horizontal and vertical MSE advection terms contribute dominantly to the propagation of the MJO MSE anomalies (second and third rows in Figure 4), closely mimicking the corresponding observations. It is worthwhile to note that the horizontal and vertical MSE advection terms appear to play a dominant role in different areas. Over the MC area, enhanced horizontal advection of MSE appears to the south of the MC islands, where the southern branch of MJO convection propagates (Figure 3). On the contrary, vertical MSE advection

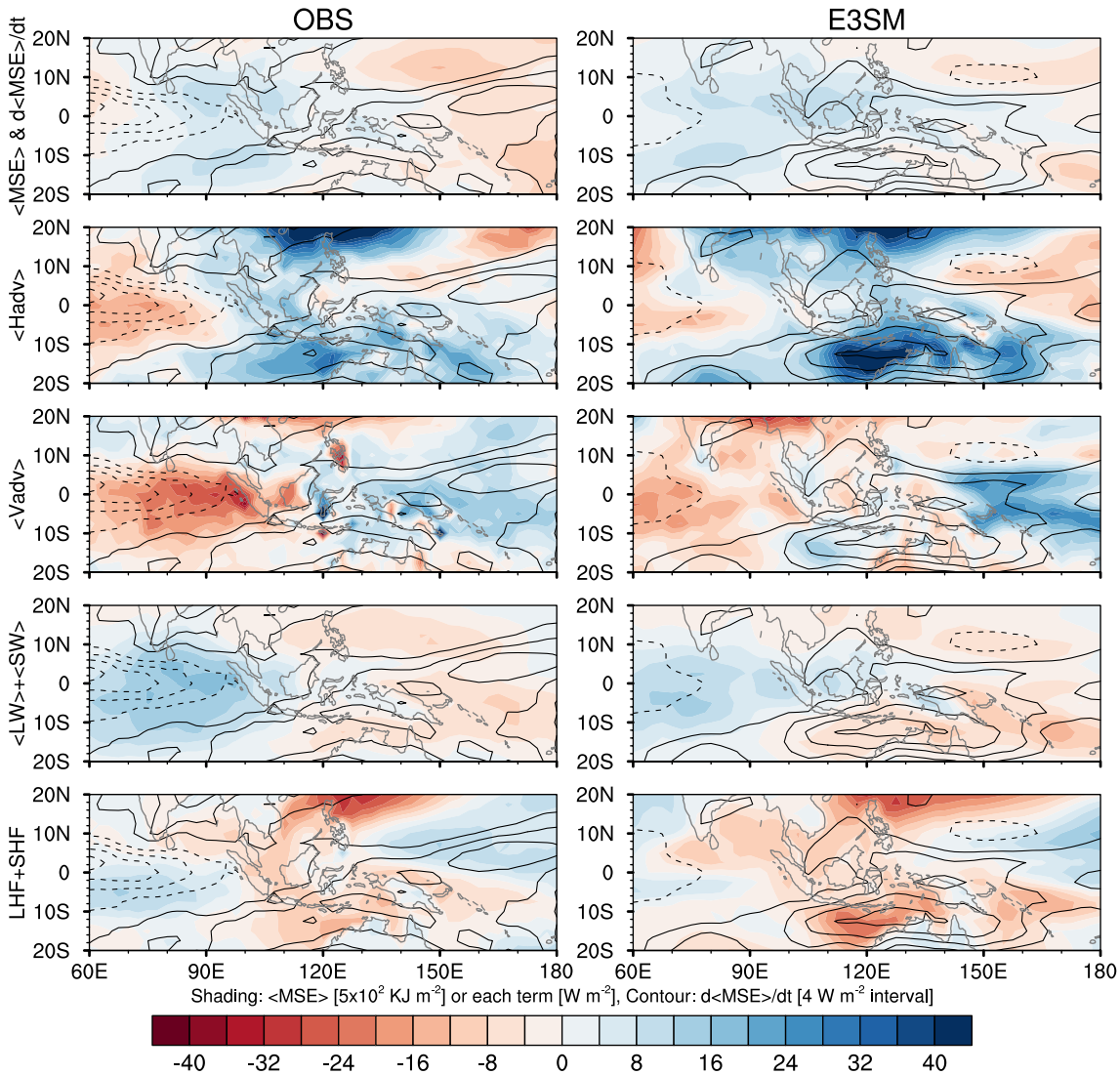

Figure 4. (first row) Column-integrated moist static energy (MSE) anomalies (kJ m^{-2}, shaded) and total MSE tendency (W m^{-2}, contour) composited for Madden-Julian oscillation phases 2 and 3: (left) ERA5 and (right) low resolution Energy Exascale Earth System Model version 1. (second to fifth rows) Same as the first row, except that shading indicates horizontal advection, vertical advection, radiative heating, and surface turbulent fluxes, respectively. The contour interval for total MSE tendency is 4 W m^{-2}.

moistens the eastern part of the MC and the western equatorial Pacific, mostly north of 5°S, where the northern branch of MJO convection prevails in later phases.

In both observations and LR E3SMv1, column-integrated radiative heating anomalies and surface turbulent heat fluxes partly compensate for the tendency by the advection terms, thereby opposing the eastward movement of the MSE anomalies (fourth and fifth rows in Figure 4). In E3SMv1, the magnitude of horizontal advection and surface latent heat flux anomalies to the south of the MC islands is larger than the observed.

Regarding the maintenance of the MJO MSE anomalies, the main balance is found between the two processes that are strongly tied to convection—vertical advection and longwave heating; longwave heating warms columns with positive MSE anomalies (Kim et al., 2015; Wolding et al., 2016), while vertical advection exports MSE out of the columns (i.e., positive gross moist stability, Neelin & Held, 1987). The opposing role of the processes is represented realistically in LR E3SMv1, although the model underestimates the magnitude of anomalous vertical MSE advection and longwave heating in the eastern Indian Ocean, where MJO convection is weaker.

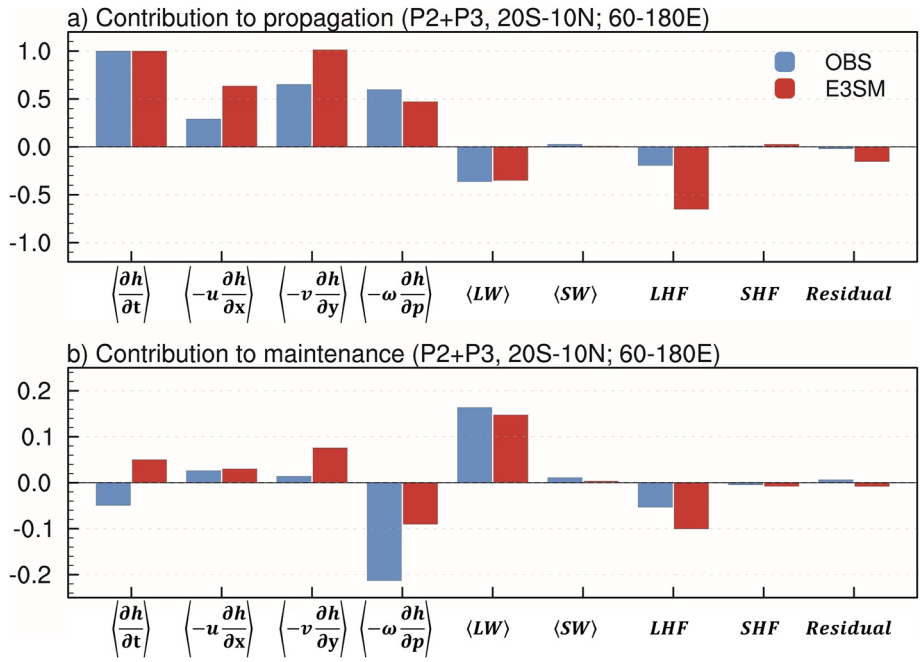

Figure 5. Contribution of each moist static energy budget term to the (a) propagation and (b) maintenance of the Madden-Julian oscillation (MJO) during Real-Time Multivariate MJO phases 2 and 3 over the Indo-Pacific warm pool (20°S–10°N and 60–180°E) during NDJFMA. Blue and red bars indicate results from observations and low resolution Energy Exascale Earth System Model version 1, respectively.

Figure 5 shows the relative contribution from each MSE budget term to the propagation of MSE anomalies, which is quantified through the pattern projection method (Equations 2a and 2b). Consistent with as indicated in Figure 4, the accelerating effect of horizontal advection and the dragging effect from latent heat flux feedback is somewhat overestimated in LR E3SMv1. The stabilizing role of vertical MSE advection is weaker than observed, while MJO MSE anomalies are overly damped by latent heat flux anomalies. To understand the model-observation discrepancy in the MJO MSE budget, the vertical structure of vertical velocity, specific humidity, and zonal wind anomalies are examined (Figure 6). Also shown in Figure 6 are the corresponding MSE and LH anomalies. While the negative latent heat flux anomalies are located slightly to the east of positive MSE anomalies in both observations and in LR E3SMv1, they are larger in magnitude and overlap more strongly with positive MSE anomalies in LR E3SMv1, indicating a stronger dragging and damping effect (LHF in Figure 5). This difference can be understood in terms of how wind anomalies are distributed around MJO convection center. Compared to observations, the westerly anomalies to the west of MJO convection are weaker, and the areas of positive MSE anomalies are more strongly dominated by easterly anomalies in the model. The easterly anomalies reduce wind speed, and hence the latent heat flux, by acting upon the climatological westerlies in the region (Figure 2). Meanwhile, the magnitude of the vertical velocity anomalies in the areas with positive MSE anomalies in the model is about 30% weaker than the observed, explaining the weaker damping effect from vertical MSE advection. The model specific humidity anomalies are muted near 850-hPa level where enhanced convection is located, in sharp contrast to ERA5, likely contributing to the weaker-than-observed vertical velocity anomalies. Note that the contribution of MSE tendency to MSE maintenance budget is not zero, indicating that the MJO MSE anomalies on average grow (LR E3SMv1) or decay (OBS) for the cases considered (MJO phases 2 and 3 with amplitude greater than 1).

Overall, LR E3SMv1 skillfully captures the observed horizontal distribution of individual MSE budget terms as well as the relative contributions to the propagation and maintenance of MJO MSE anomalies. The results for the other MJO phases are similar (not shown).

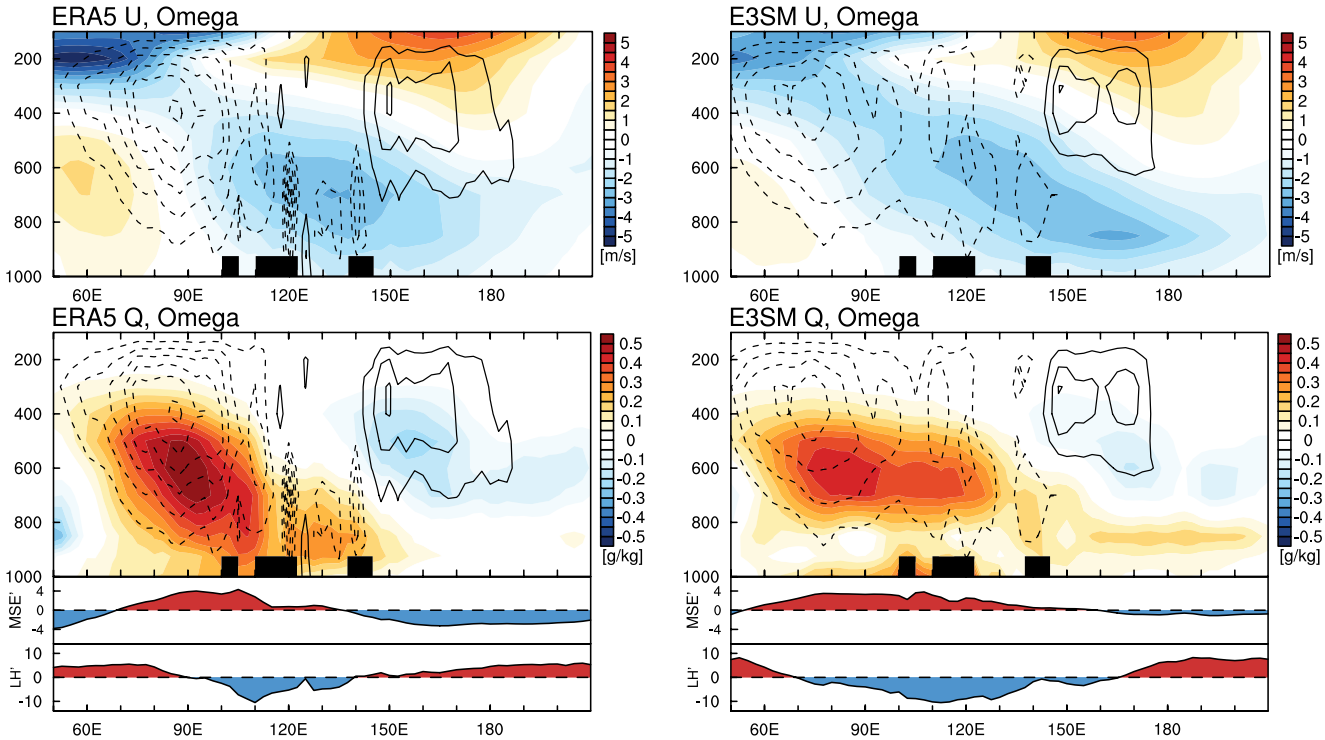

Figure 6. (top) Intraseasonal zonal wind (m s^{-1}, shaded) and pressure velocity (Pa s^{-1}, contour) anomalies averaged over the equatorial band (10°S–10°N) composited for Madden-Julian oscillation phases 2 and 3: (left) ERA5 and (right) low resolution Energy Exascale Earth System Model version 1. (bottom) Same as the top panels, except for intraseasonal specific humidity anomalies (g kg^{-1}) are shaded. The contour interval for pressure velocity is 0.005 Pa s^{-1}. Line graphs at the bottom indicate column-integrated intraseasonal moist static energy ($\times 10^4$ kJ m^{-2}) and latent heat flux (W m^{-2}) anomalies.

4.4. Modulation of MC Diurnal Cycle by the MJO

Many recent observational and modeling studies focused on the role of the diurnal cycle of convection in the MC islands on the propagation of the MJO (e.g., Hagos et al., 2016; Zhang & Ling, 2017). It was hypothesized that strong convection over the MC islands associated with the diurnal cycle could inhibit oceanic convection nearby and hence block MJO propagation (Zhang & Ling, 2017). Because anomalous convection associated with the MJO develops mainly over water (Sobel et al., 2008, 2010), suppression of MC oceanic convection during MJO phases 3 and 4 could terminate an MJO event.

Figure 7 displays the amplitude and phase of the precipitation diurnal cycle in observations and in LR and HR E3SMv1, which are obtained by projecting the composite diurnal cycle of precipitation onto the diurnal harmonics in each grid point as in Peatman et al. (2014). LR E3SMv1 shows the biases in the diurnal cycle of precipitation in the MC region that are common to many global climate models (GCMs; Baranowski et al., 2019; Tang et al., 2021; Xie et al., 2019): it underestimates the amplitude of the diurnal cycle while the peak phase of the diurnal cycle occurs too early. The peak amplitude of the diurnal cycle in the model is less than 50% of what TRMM observations suggest. The weaker-than-observed diurnal cycle amplitude over MC islands might explain why the apparent MC damping effect on the MJO is less pronounced in LR E3SMv1 (Figure 1). The time of maximum diurnal precipitation occurs a few to several hours earlier in the model than in observations over water and the islands. It is worthwhile to mention the difference in phasing of the diurnal cycle between LR E3SMv1 (a coupled simulation, Figure 7e) and the control simulation made with LR EAMv1 (an uncoupled simulation; Figure 12b in Xie et al., 2019); the peak diurnal rain seems to occur a few hours later in LR E3SMv1 over the islands than in LR EAMv1. This might suggest that air–sea coupling or the mean state changes due to coupling could affect the diurnal cycle timing phase. It is also possible that the parameter tuning conducted before freezing the coupled version (Table 1 in Golaz et al., 2019) have affected the simulation of the diurnal cycle. The systematic bias in the diurnal cycle amplitude is partly alleviated in HR E3SMv1, presumably because it better resolves the complex land–sea contrast and steep topography in the region (Figure 7).

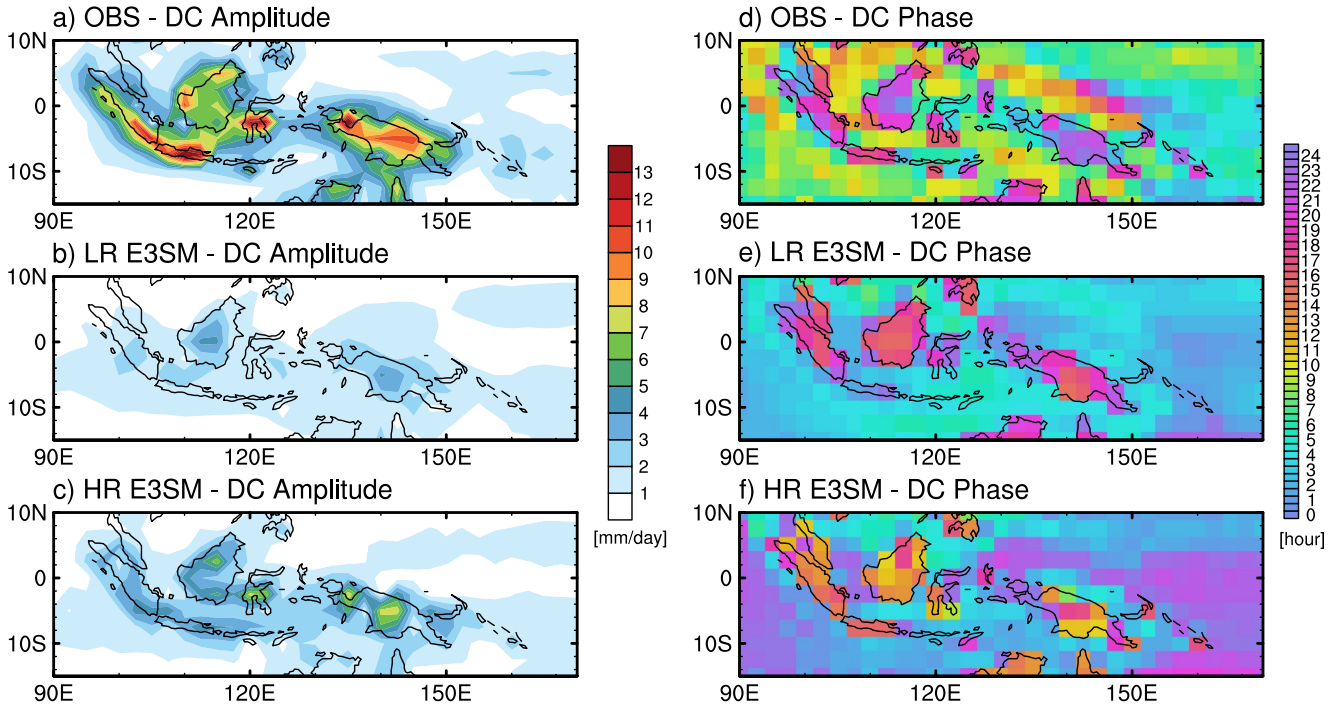

Figure 7. Climatological (left) amplitude (mm day^{-1}) and (right) phase (hour) of the diurnal harmonic of precipitation from (top) Tropical Rainfall Measuring Mission, (middle) low resolution Energy Exascale Earth System Model version 1 (E3SMv1), and (bottom) high resolution E3SMv1 during NDJFMA.

Although still too weak, the diurnal cycle amplitude almost doubles in HR E3SMv1 when compared to the LR version. HR E3SMv1 experiences more pronounced MJO MC barrier effect (Figure 1), possibly due to the stronger mean MC diurnal cycle. However, the peak phase of the diurnal cycle in HR E3SMv1 is even earlier than in LR E3SMv1, suggesting that factors other than grid size may affect the phasing of the diurnal cycle.

The modulation of the diurnal cycle of precipitation in the MC region by the MJO has been examined using satellite observations (e.g., Figure 7 in Peatman et al., 2014). Despite the biases in the amplitude and phase of the diurnal cycle, LR and HR E3SMv1 reasonably capture the modulation of the diurnal cycle amplitude by the MJO (Figure 8), especially over relatively big islands (Borneo and New Guinea), with the diurnal cycle being enhanced when the MJO's main convection center is located in the Indian Ocean (phases 1–3) and western MC (phase 4). As in observations, the enhancement of the diurnal cycle appears to contribute to the vanguard precipitation anomalies (Figure 3) in phases 1 and 2. Presumably due to the coarse horizontal resolution, the modulation of the diurnal cycle by the MJO is most pronounced in the center of the islands in LR E3SMv1, whereas in observations, and to a lesser degree in HR E3SMv1, it is most pronounced in the coastal areas in Sumatra, Java, and Borneo and over the entire island in Sulawesi and New Guinea, again showing the benefit of employing a finer grid spacing on resolving the diurnal cycle of precipitation in the region.

Figure 9 shows the average evolution of oceanic and land precipitation in the western MC area (15°S–10°N, 100°–120°E) as functions of the local time and the MJO phase. The MJO affects the diurnal cycle of MC land and oceanic convection mostly by changing the amplitude of the diurnal cycle, whereas its impact on the phase of the diurnal cycle (i.e., the local time when the diurnal precipitation peaks) is minimal. That is, precipitation composites exhibit substantial changes in their strength by MJO phases while their peaks remain around the same local time. Figure 9 also shows that oceanic precipitation peaks during MJO phases 4 and 5 while land precipitation maxima take place about 1 and 2 phases earlier, with the ratio of oceanic to land precipitation being the largest at MJO phase 5.

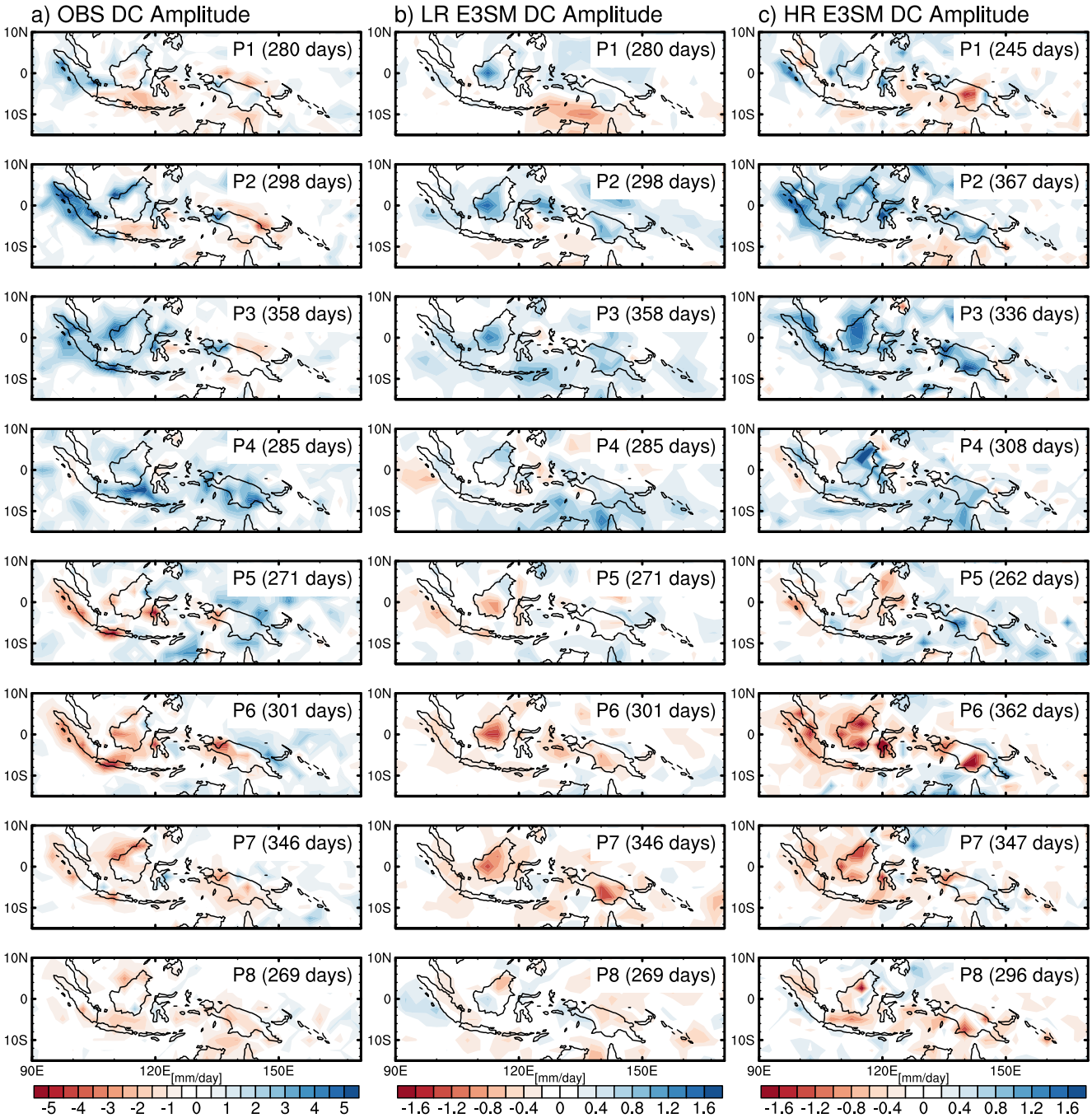

Figure 8. Madden-Julian oscillation (MJO) life cycle composite maps of anomalous diurnal harmonic amplitude of precipitation (mm day^{-1}) obtained from each Real-Time Multivariate MJO phase during NDJFMA: (a) Tropical Rainfall Measuring Mission, (b) low resolution Energy Exascale Earth System Model version 1 (E3SMv1), and (c) high resolution E3SMv1.

4.5. MJO Teleconnections

Observational evidence (e.g., Weickmann, 1983) and theoretical understanding (e.g., Hoskins & Karoly, 1981) of the MJO's influence on the extratropical circulation were established in the early 1980s (reviews on this topic are available in Stan et al., 2017 and Jiang et al., 2020). The systematic fluctuations of midlatitude circulation associated with the MJO are understood as the anomalous rotational flow excited by the MJO 'Rossby wave source' (Sardeshmukh & Hoskins, 1988), which then propagate through the medium of the extratropical basic state as a stationary Rossby wave packet (Hoskins & Karoly, 1981; Hoskins & Ambrizzi, 1993).

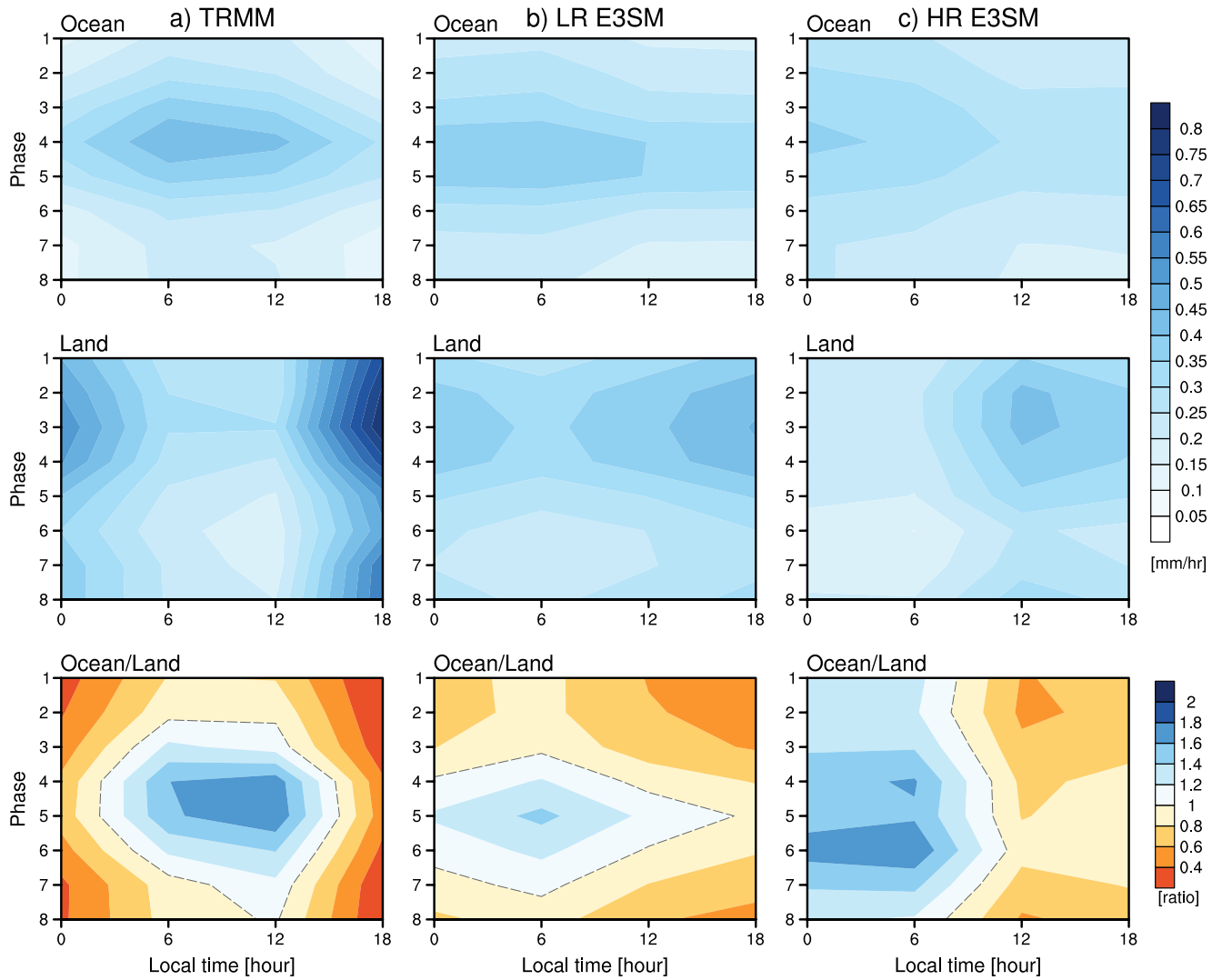

Figure 9. Composite diurnal cycle of (upper) oceanic and (middle) land precipitation (mm day^{-1}) and (lower) their ratio over the western Maritime Continent (15°S–10°N, 100–120°E) as a function of adden-Julian oscillation phase: (a) Tropical Rainfall Measuring Mission and (b) low resolution Energy Exascale Earth System Model version 1 (E3SMv1), and (c) high resolution E3SMv1.

Consistent with the theoretical understanding, modeling studies of MJO teleconnections emphasized both accurate representation of MJO diabatic heating (Yoo et al., 2015; Stan & Straus, 2019) and realistic extratropical basic state (Henderson et al., 2017) as key aspects for GCMs to correctly capture the circulation changes associated with the MJO. Because the two factors—MJO variability and the mean state—often show tradeoffs with conventional cumulus parameterization schemes (Kim et al., 2011; Mapes & Neale, 2011), modeling MJO teleconnection presents a challenging problem for any GCM. MJO teleconnections in the contemporary GCMs are often too strong, too persistent, and extended too far to the east (Wang et al., 2020a). Also, for the MJO's modulation of the PNA pattern (e.g., Mori & Watanabe, 2008), the latitudinal position, zonal extent, and intensity of the Pacific subtropical jet show some robust relationship with the skill scores for MJO teleconnection in the models (Wang et al., 2020b).

Figure 10 shows 500-hPa geopotential height (Z500) anomalies (shaded) for four selected MJO phases in observations (left), the LR (middle) HR (right) simulations, together with the mean state 300-hPa zonal wind (green contours). The geopotential height anomalies are averaged between 5 and 9 days after the days with a strong MJO signal (amplitude >1). The Pacific subtropical jet is reasonably represented in both E3SMv1 simulations, although it is shifted slightly southward in LR E3SMv1, especially in the central Pacific. In observations, a negative

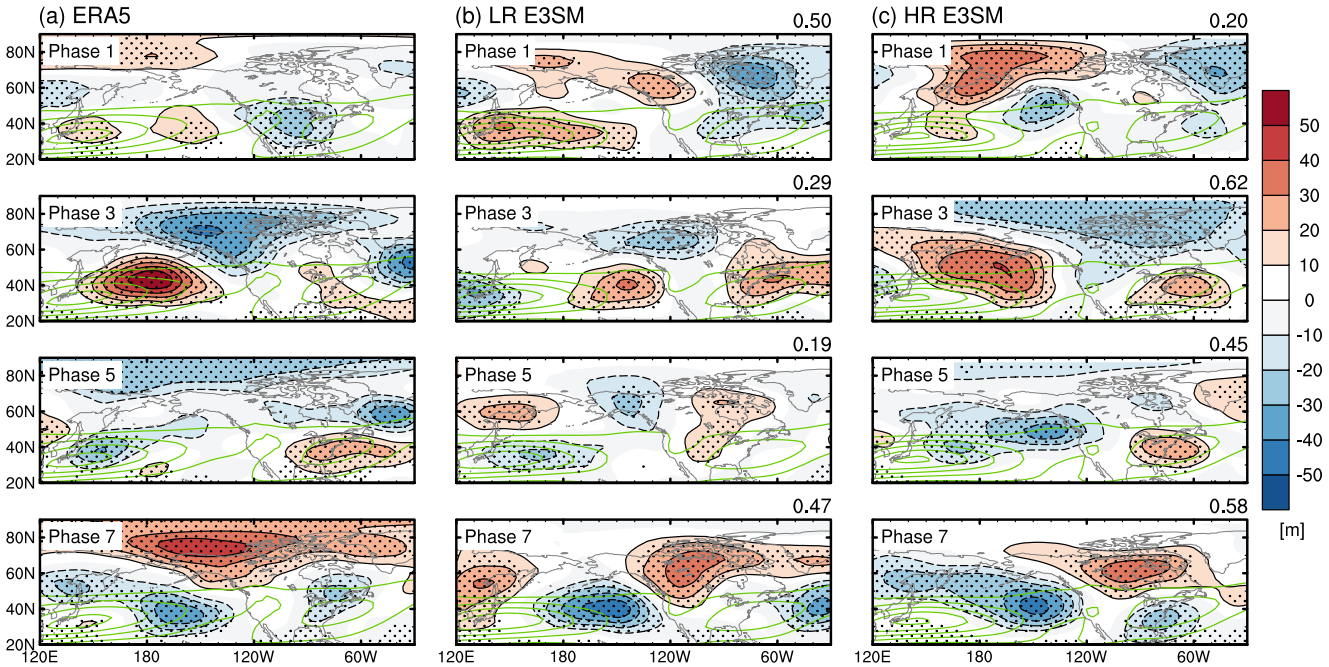

Figure 10. Madden-Julian oscillation (MJO) life cycle composite maps of 5–9 days average 500-hPa geopotential height anomalies (m, shaded) obtained from the selected four Real-Time Multivariate MJO phases during NDJFMA. Green contours indicate the climatological 300-hPa zonal wind (m s^{-1}, contour interval: 10 m s^{-1}). Green contours begin from 20 m s^{-1}. (a) ERA5, (b) low resolution Energy Exascale Earth System Model version 1 (E3SMv1), and (c) high resolution E3SMv1. The geopotential height anomalies that are statistically significant at the 95% confidence level are indicated by the dots. For E3SM simulation results, the pattern correlation with the observed anomalies over the domain covered by figures (20–90°N, 120–330°E) is indicated at the right top of each panel.

and positive PNA pattern appears after MJO phases 3 and 7, respectively, which is realistically captured by both LR and HR E3SMv1 simulations. Interestingly, HR E3SMv1 seems to perform better in terms of the pattern and magnitude of MJO-associated Z500 anomalies, despite precipitation anomalies associated with the MJO in HR E3SMv1 being weaker than in LR E3SMv1. The pattern correlations with the observed Z500 anomalies are overall higher in HR E3SMv1, except for the phase 1 result. The lead-lag relationship of PNA-like circulation anomalies with the MJO phases are also more realistically simulated in HR than in LR (Figure 11), suggesting that a finer grid spacing might be beneficial for a model to simulate the MJO teleconnections. For MJO phases

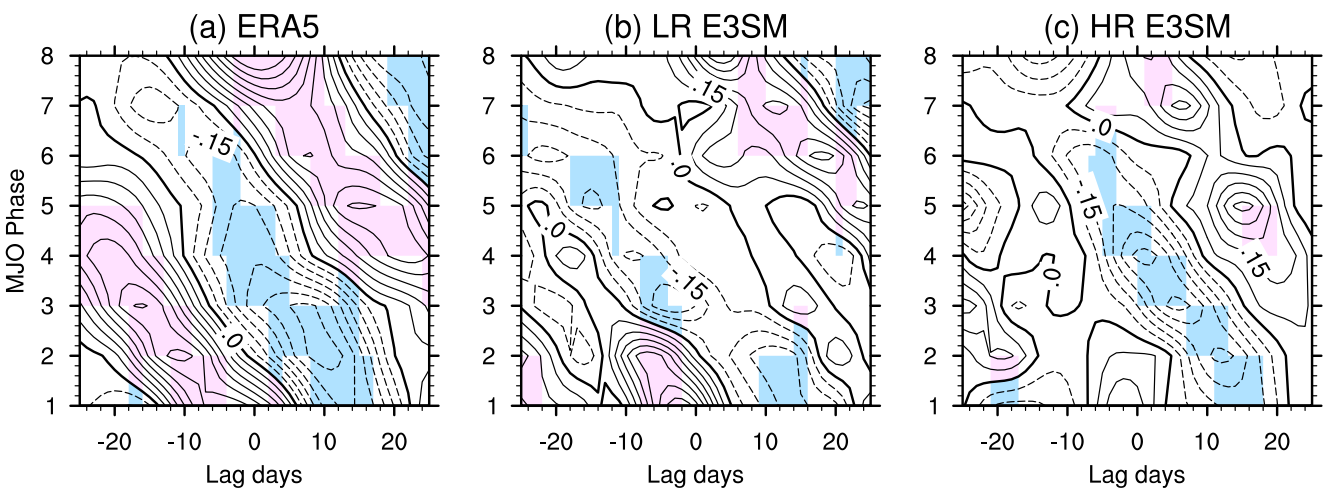

Figure 11. Lead-lag composite of the Pacific North American index around strong Madden-Julian oscillation (MJO) days for each MJO phase during NDJFMA: (a) ERA5, (b) low resolution Energy Exascale Earth System Model version 1 (E3SMv1), and (c) high resolution E3SMv1. Pink and blue shading indicates that positive and negative composite values are statistically significant at the 95% confidence level.

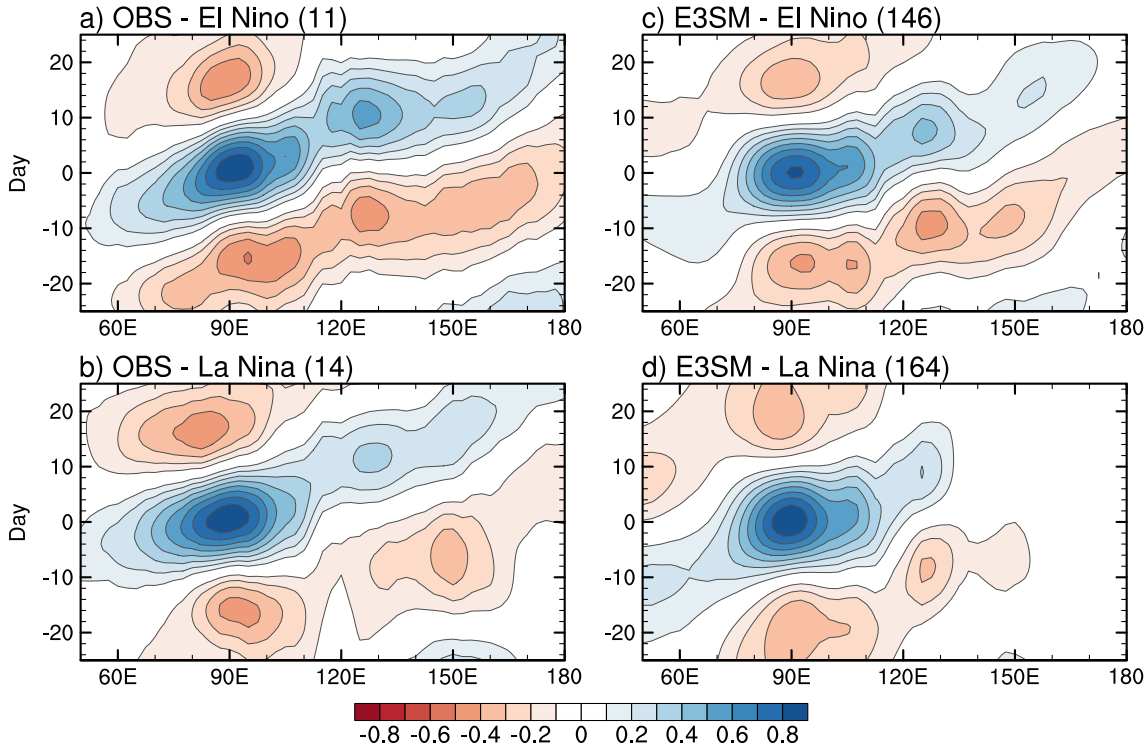

Figure 12. Longitude–lag diagram of equatorial (10°S–10°N) outgoing longwave radiation (OLR) regressed against intraseasonal OLR anomalies in the Indian Ocean reference region (5°S–5°N, 85–95°E) during DJF for the El Niño and La Niña years from (left) observations and (right) 5-ensemble CMIP6 Historical simulation made with low resolution Energy Exascale Earth System Model version 1 (LR E3SMv1). Numbers in parentheses denote the number El Niño and La Niña years. For observations and LR E3SMv1, El Niño and La Niña years are defined as the years with sea surface temperature anomalies averaged over the Niño3.4 region (5°S–5°N, 170–120°W) being higher than its 0.5 standard deviation and lower than its −0.5 standard deviation, respectively.

1 and 5, the observed Z500 anomalies are weaker than those for the other MJO phases (Tseng et al., 2019). The model-observation agreement is also low during phases 1 and 5 compared to that for phases 3 and 7, except for the eastern US for phase 5, in which HR E3SMv1 correctly captures the anomalous high.

4.6. Interannual Variability of the MJO

We investigate in this subsection the modulation of MJO propagation characteristics by ENSO and QBO by utilizing the 5-member ensemble historical simulation made with LR E3SMv1. Note that the analysis in this subsection is limited to DJF.

4.6.1. ENSO-MJO

Many studies have examined how ENSO affects the MJO in the past few decades (e.g., Slingo et al., 1999). In observations, MJO propagation tends to be damped more strongly over the MC region in La Niña years (e.g., DeMott et al., 2018; Gonzalez & Jiang, 2019; Gushchina & Dewitte, 2012; Kang et al., 2021; Klingaman & Demott, 2020; Tam & Lau, 2005; Wei & Ren, 2019). Figure 12 shows that to the east of around 110°E the MJO OLR anomalies are much weaker during the La Niña years than in El Niño years. This contrast between El Niño and La Niña years is realistically captured in E3SMv1, showing that the MJO propagates farther to the east during the El Niño years.

Recent studies have emphasized the role of the mean state moisture gradient on the propagation of the MJO (e.g., DeMott et al., 2018; Kang et al., 2021; Klingaman & Demott, 2020). While detailed moisture budget analysis is not possible with the long-term historical simulation due to the unavailability of the required variables, Figure 13 offers clues on how the SST changes associated with ENSO can affect MJO variability. During El Niño years compared to La Niña years, the tropical Pacific Ocean experiences anomalously high SST near the equator and associated PW anomalies that are straddled by weaker cold SST and dry PW anomalies in the off-equatorial

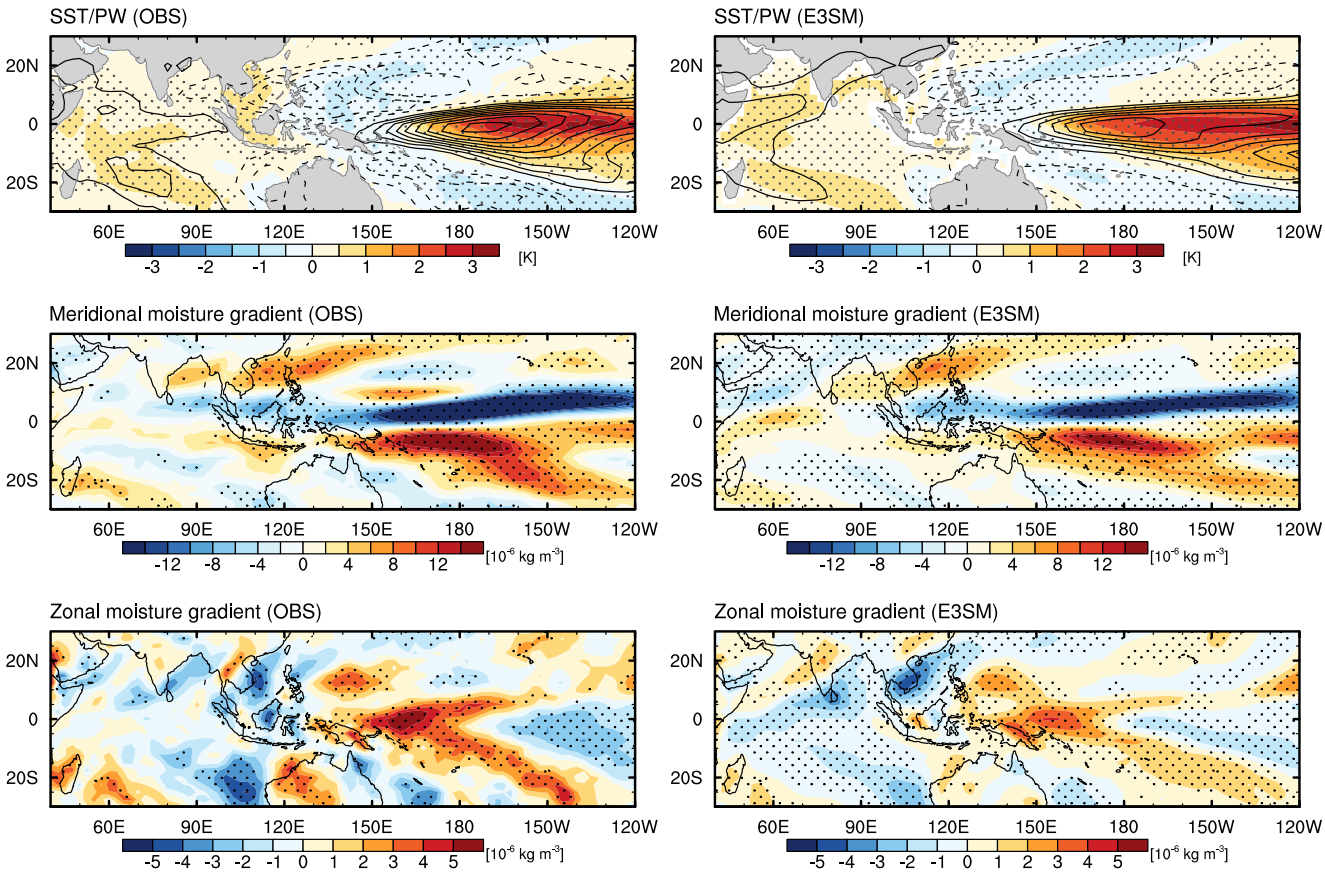

Figure 13. Differences between the El Niño and La Niña years in DJF mean state: (left) observations and (right) 5-ensemble CMIP6 Historical simulation made with low resolution Energy Exascale Earth System Model version 1 (LR E3SMv1). (top) Sea surface temperature (K, shaded) and precipitable water (PW; kg m^{-2}, contour), (middle) meridional and (bottom) zonal gradient of PW ($\times 10^{-6}$ kg m^{-3}). Black dots indicate the differences are statistically significant at the 95% confidence level. For observations, 11 El Niño and 14 La Niña years were used, while 146 El Niño and 164 La Niña years were used for LR E3SMv1.

western and central Pacific. This pattern of PW anomalies steepens meridional gradient on both sides of the equator in the MC and west Pacific (Figure 13, second row). A steeper mean state meridional moisture gradient would lead to a larger meridional moisture advection per unit meridional wind anomalies, promoting enhanced moisture recharging to the east of the MJO (Ahn, Kim, Kang, et al., 2020; Ahn, Kim, Ham, et al., 2020; DeMott et al., 2019; Jiang, 2017; Kang et al., 2021). Also, the ENSO-associated PW anomalies weaken the climatological negative zonal moisture gradient in the western Pacific (Figure 13, third row). With the weaker negative zonal moisture gradient, the drying caused by MJO easterly anomalies to the east of MJO convection would be weaker during El Nino years compared to La Nina years, meaning that the basic state environment that is favorable for MJO is extended farther to the east. The E3SMv1 results support the notion that ENSO affects MJO by modulating the mean state moisture gradient.

4.6.2. QBO-MJO

Figure 14 compares MJO propagation characteristics between the easterly and westerly phases of QBO (EQBO and WQBO, respectively, hereafter). The propagation of the MJO during EQBO years is stronger and covers a wider zonal range than during WQBO years in observations (e.g., Son et al., 2017; Yoo & Son, 2016). As in many other contemporary climate models, the MJO in E3SMv1 exhibits no sensitivity to the QBO, with MJO propagation characteristics being almost identical between EQBO and WQBO years (Figure 14), despite the zonal mean temperature response to QBO in the upper troposphere and lower troposphere is realistically represented in E3SMv1 (Figure 15). We also examined the QBO–MJO relationship in the recent decades to see if the relationship emerges with the greenhouse gas-induced warming (Klotzbach et al., 2019). Our results showed that while the model could capture the lower stratospheric cooling in the recent decades, there was no notable trend in the QBO–MJO relationship (not shown). The lack of the QBO–MJO relationship in E3SMv1 might be due to the

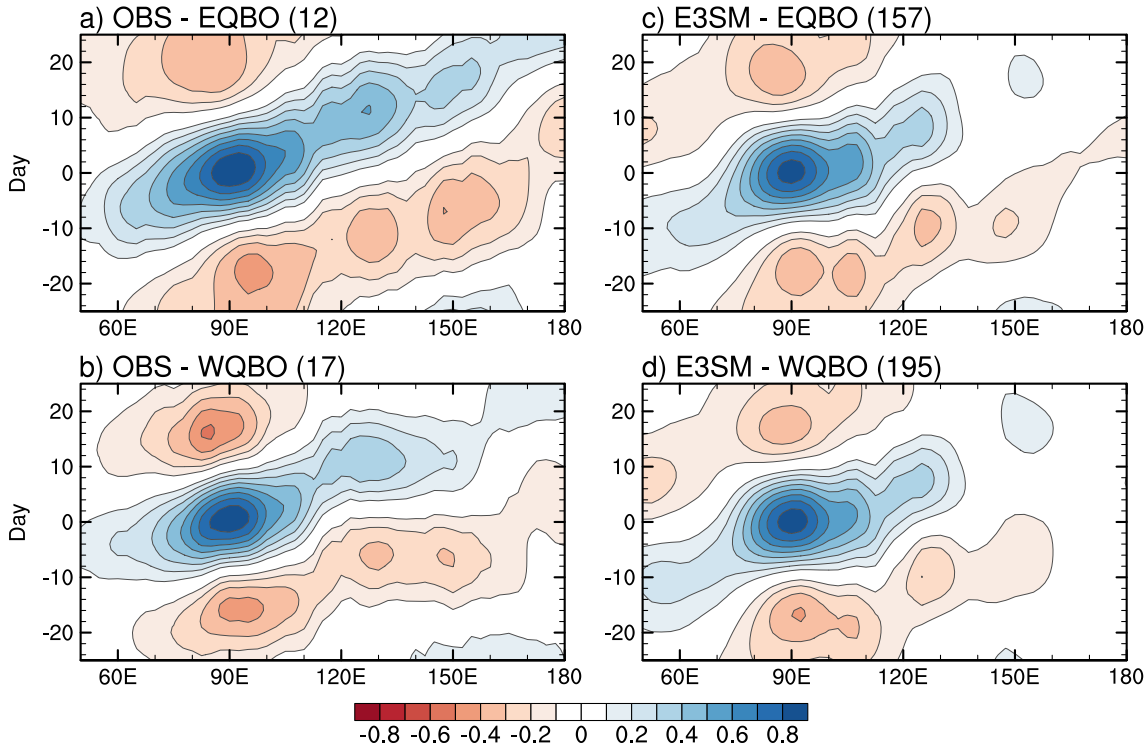

Figure 14. Same as Figure 12, except for the (top) EQBO and (bottom) WQBO years obtained as the years with 50-hPa zonal wind anomalies averaged in the equatorial band (10°S–10°N) being lower than −0.5 standard deviation and higher than 0.5 standard deviation.

bias in the representation of the QBO, which is too fast and too strong compared to the observed QBO variability (Richter et al., 2019). Hendon and Abhik (2018) proposed a hypothesis that the zonal mean temperature anomaly associated with the QBO affects the MJO by modulating the strength of the cold cap above MJO convection. During EQBO years, the cold cap becomes stronger and provides enhanced positive feedback to anomalous

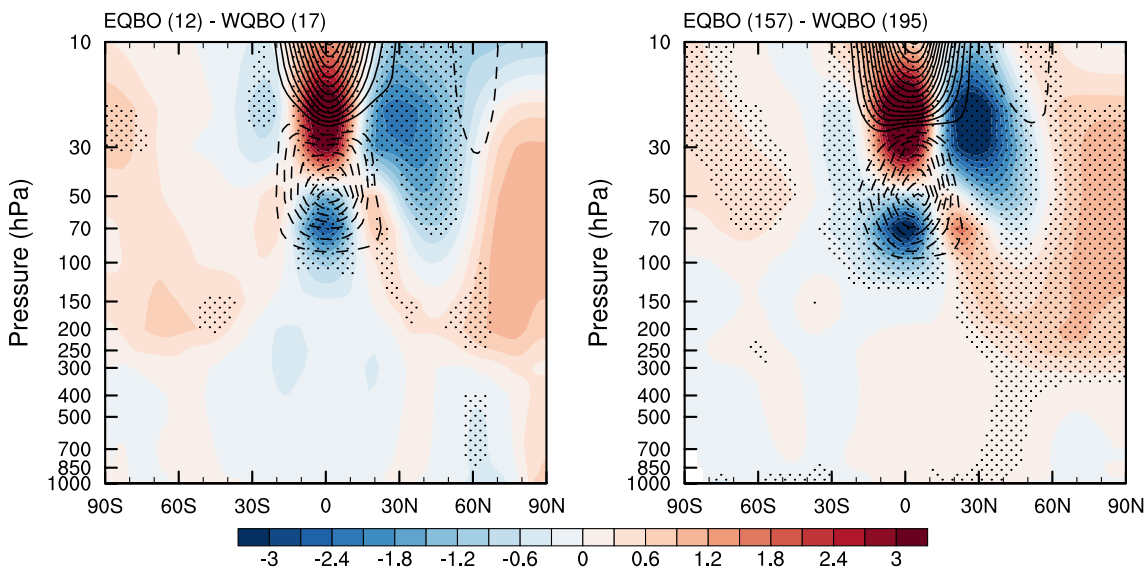

Figure 15. Differences between the EQBO and WQBO years in DJF-mean zonal-mean temperature (K, shaded) and zonal wind (m s^{-1}, contour): (left) observation and (right) 5-ensemble CMIP6 Historical simulation made with low resolution Energy Exascale Earth System Model version 1. The contour interval is 3 m s^{-1} and solid and dashed contours indicate positive and negative anomalies, respectively. Zero line is omitted. Black dots indicate shaded differences are statistically significant at the 95% confidence level.

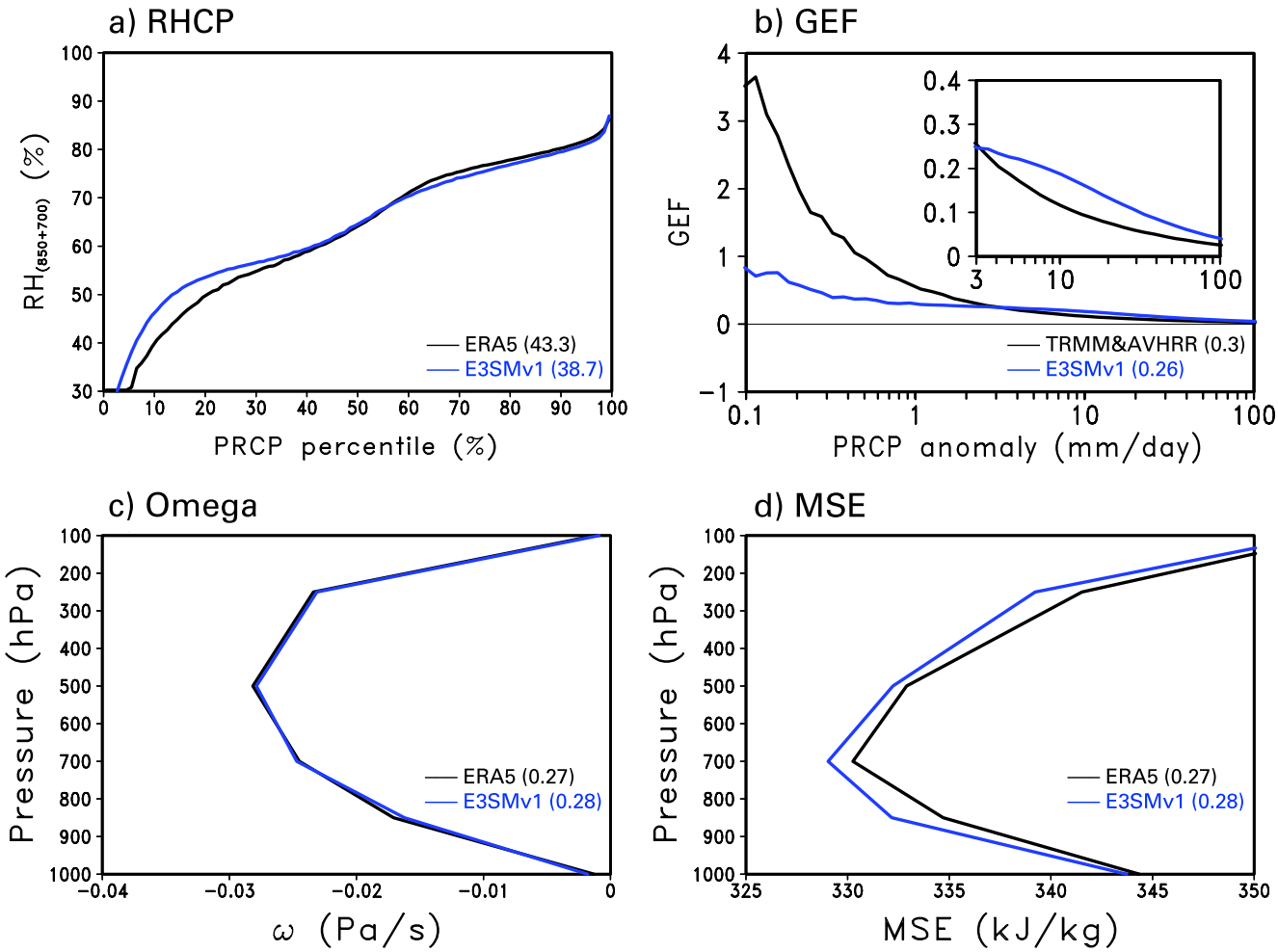

Figure 16. Process-oriented Madden-Julian oscillation diagnostics: (a) the relative humidity composite based on precipitation percentile (RHCP, %), (b) the greenhouse enhancement factor (GEF, unitless), and the vertical profiles of the mean state (c) pressure velocity (Pa s^{-1}) and (d) moist static energy (MSE, kJ kg^{-1}) from observations (black) and low resolution Energy Exascale Earth System Model version 1 (blue). The pressure velocity and MSE profiles are used for the calculation of normalized gross moist stability (NGMS). The Indo-Pacific warm pool area (60−180°E, 15°S–15°N) excluding land grid points is used for all the process-oriented diagnostics. Numbers in parentheses next to data labels denote the process-oriented metric values of RHCP, GEF, and NGMS.

convection, aiding further development. If the model convection scheme is not sensitive enough to the changes in the upper tropospheric and lower stratospheric static stability, it is possible that the parent model is unable to simulate the QBO–MJO relationship even with realistic representations of both.

4.7. Process-Oriented MJO Diagnostics

In this section, we present results from selected process-oriented MJO diagnostics that are designed to offer insights into the process-level bias of the model that may affect its MJO simulation fidelity. Many process-oriented MJO diagnostics focus on the moist thermodynamics in the atmosphere, in particular, the interaction among moisture, convection, cloud, and radiation. For the tropical oceans, the amount of rain over a large area is strongly tied to how saturated the column is (Bretherton et al., 2004; Peters & Neelin, 2006; Rushley et al., 2018), which leads to a sharp contrast in rain rate between dry and wet columns. Kim, Xavier, et al. (2014) and Kim, Kug, and Sobel (2014) proposed the relative humidity composite based on precipitation (RHCP) diagnostic to quantify the strength of the coupling between moisture and precipitation. The RHCP diagnostic displays the lower free-tropospheric RH (average of 850-hPa RH and 700-hPa RH) as a function of precipitation percentile. Figure 16a shows that the model RH is close to the reference (ERA5) overall, although slightly underestimated in the low precipitation percentiles. The precipitation–moisture coupling in the model measured as the RH difference between

columns with high (upper 10%) and low (lower 20%) rain rate—the RHCP metric, which is shown to be positively correlated with MJO performance metrics (e.g., Ahn et al., 2017; Jiang et al., 2015; Kim, Kug, & Sobel, 2014; Kim, Xavier, et al., 2014;) is slightly weaker than in ERA5 (38.7% vs. 43.3%), suggesting that enhancing moisture sensitivity of convection in the model may lead to a stronger MJO (e.g., Kim et al., 2012).

The longwave cloud-radiation feedback has been suggested as the dominant maintenance mechanism of the MJO in many observational and model studies (e.g., Andersen & Kuang, 2012; Lin & Mapes, 2004; Sobel et al., 2014). One way of quantifying the strength of the longwave cloud-radiation feedback is by assessing the ratio between OLR and precipitation anomalies in the same unit, as an approximation to the ratio between anomalous column-integrated longwave and condensational heating. Figure 16b displays the ratio as a function of precipitation anomaly on a log scale, which is referred to as the Greenhouse Enhancement Factor (GEF) diagnostic in Kim et al. (2015). It was also shown in Kim et al. (2015) that the ratio for the weak-to-moderate rain rate anomalies (1–5 mm day^{-1})—the GEF metric—exhibited a statistically significant positive correlation with MJO performance measures. LR E3SMv1 underestimates the GEF for precipitation anomalies lower than 3 mm day^{-1}, while overestimating it for higher intensity precipitation anomaly bins (Figure 16b). While the GEF metric from LR E3SMv1 is close to the reference value (0.26 vs. 0.3), the role of the weaker-than-observed GEF for the columns with weak precipitation anomalies on MJO variability in the model warrants further investigation. Recent studies found that the MJO is distinguished from other convectively coupled waves in the tropics by the fact that it is destabilized by longwave cloud-radiation feedback (Inoue et al., 2020; Sakaeda et al., 2020). Considering the perceived role of the longwave cloud-radiation feedback on the observed MJO–QBO relationship (e.g., Sakaeda et al., 2020), it will be also of great interest to revisit the MJO–QBO coupling in a version of the model with stronger GEF.

The normalized gross moist stability (NGMS, Raymond et al., 2009) is a measure of how efficiently a column can export anomalous energy that goes into it through its boundaries (Neelin & Held, 1987). It has been shown that models with a lower NGMS, hence less stable to energy input, tend to simulate stronger intraseasonal variability and MJO (e.g., Benedict et al., 2014). Ahn et al. (2017) estimated the NGMS as the ratio between column-integrated vertical MSE advection to column-integrated vertical dry static energy (DSE) advection using the time-averaged and warm pool-averaged vertical profiles of MSE, DSE, and pressure velocity. They showed that the resulting NGMS metric is negatively correlated with MJO performance measure. Figure 16c show that warm pool averaged pressure velocity from LR E3SMv1 closely matches that from ERA5. In the MSE profile (Figure 16d), the overall shape is realistically captured in LR E3SMv1, despite the MSE value is lower than the observed throughout the troposphere associated with the dry bias (Figure 2). Nonetheless, the model NGMS obtained from the time-averaged and warm pool-averaged profiles is close to the value from ERA5 (0.27 vs. 0.28), indicating that one metric—NGMS in this case—is not enough to characterize the simulated mean state. In the model development point of view, it will be of interest whether the dry bias can be alleviated without deteriorating the vertical profile of the mean MSE.

5. Summary and Conclusions

The MJO, the dominant source of Earth system predictability at the intraseasonal time scale, is a known driver of many types of extreme events all over the globe. However, an accurate representation of the MJO and its teleconnections is still one of the most challenging tasks for many GCMs. In the current study, we documented the performance of the DOE's new Earth system model—the E3SMv1 in simulating MJO variability and its teleconnections. Simulations made with low (~100-km, LR) and high (~25-km, HR) resolution versions of E3SMv1 were analyzed with respect to their mean states (Section 4.1), MJO propagation characteristics (Section 4.2), MJO MSE budgets (Section 4.3), MJO interactions with MC islands (Section 4.4), MJO teleconnections to the midlatitudes (Section 4.5), and MJO regulation by interannual variability (Section 4.6). In addition, selected process-oriented MJO diagnostics were applied to the LR E3SMv1 (Section 4.7).

We found that LR and HR E3SMv1 adequately simulate the eastward propagation of the MJO over the Indo-Pacific warm pool (Figure 1), despite MJO convection anomalies being weaker in the Indian Ocean (Figure 3), which is presumably due to the bias in the mean state moisture (Figure 2). Interestingly, the widespread dry bias over the Indo-Pacific warm pool (Figure 2) does not severely affect the model's fidelity to simulate the eastward

propagation of the MJO, suggesting either that the model mean state biases are not critical to MJO simulation or that the effect of the mean state bias is compensated by errors in other aspects of the model simulation.

It was shown that MJO precipitation anomalies in LR E3SMv1 were tightly coupled to column-integrated MSE anomalies (Figure 3), suggesting that moisture dynamics play a key role in their maintenance and propagation. The pattern and magnitude of individual MSE budget terms associated with the MJO in LR E3SMv1 closely mimic those in observations (Figures 4 and 5). The MSE budget highlighted that horizontal moisture advection and longwave radiative feedback were key processes that led to the eastward movement and maintenance of MSE anomalies in the model, respectively. Despite our finding that the mean state zonal and meridional moisture gradient is weaker in the model than in observations (Figure 2), horizontal advection of MSE drives the MJO's eastward propagation more strongly in the model than in observations, due to the stronger-than-observed MJO wind anomalies in the model (Figure 5). On the other hand, the damping and dragging effects from latent heat flux feedback were found to be overestimated in the model, likely due to the bias in the wind-convection relationship (Figure 6). One contributing factor might be the underestimation of latent heat fluxes in the LR E3SMv1 surface flux parameterization in low wind conditions. This known deficiency has been partly alleviated in other versions of E3SM (e.g., Harrop et al., 2018) by using a "gustiness parameterization" that makes the surface fluxes sensitive to estimates of parameterized subgrid processes (convection, and turbulence).

The LR and HR E3SMv1 exhibited systematic biases in the magnitude and phase of the diurnal cycle of precipitation in the MC region that are common to many other contemporary GCMs; the diurnal variation of precipitation was too weak, and it peaked a few to several hours earlier than observed (Figure 7). Despite the systematic biases, however, we found that the modulation of the diurnal cycle of precipitation in the MC region by the MJO was realistically captured in E3SMv1 (Figures 8 and 9), indicating that the model handles the interactions between large-scale MJO circulation and small-scale convective systems over the MC region in a realistic manner. The weak diurnal cycle over the MC islands in LR E3SMv1 might have contributed to the weaker-than-observed MC barrier effects on MJO (Figure 1), by facilitating the development of oceanic convection (Hagos et al., 2016; Zhang & Ling, 2017).

The LR and HR E3SMv1 also reasonably captured the pattern and magnitude of circulation anomalies in the PNA region while the magnitude was a bit weaker than the observed, especially for MJO phases 3 and 7 (Figure 10). On the other hand, the model representation of MJO teleconnection poorly matched the observed for MJO phases 1 and 5, when the teleconnection is relatively weak and less coherent in the PNA region. Interestingly, the HR E3SMv1 appeared to perform better than the LR version in terms of the MJO–PNA relationship (Figure 11), suggesting that better resolving small-scale eddies in the midlatitude might help improve MJO teleconnection.

As in observations, the zonal extent of the MJO's eastward propagation was strongly modulated by ENSO in LR E3SMv1 (Figure 12). During El Niño years compared to La Niña years, the mean state moisture gradient in the tropical west Pacific changed to favor more effective moisture recharging by horizontal moisture advection to the east of MJO convection, facilitating further eastward propagation of MJO (Figure 13). Our results support recent observational and modeling studies that emphasized the role of the mean state moisture gradient as the critical feature of the mean state for the MJO's propagation.

On the contrary, LR E3SMv1, like many other contemporary GCMs, was found to be unable to capture the strong coupling between MJO and the stratospheric QBO; MJO propagation characteristics showed no difference between the easterly QBO and westerly QBO years (Figure 14). The lack of the QBO–MJO coupling in E3SMv1, which realistically simulates the temperature changes associated with QBO in the upper troposphere and lower stratosphere (Figure 15), might suggest that the model convection and cloud parameterizations are missing an important process that is critical for convection to be sensitive to circulation changes in the upper troposphere and lower stratosphere. Another possibility is that the QBO influence on MJO variability is hindered because the model QBO oscillates too fast (Richter et al., 2019), making it difficult for the QBO-associated circulation changes to serve as the background conditions for MJO. Richter et al. (2019) showed that the bias in QBO periodicity and amplitude can be alleviated by tuning two key parameters in the gravity wave parameterization scheme. It will be of great interest to re-visit the MJO–QBO relationship in a future version of E3SM, in which the modified gravity wave parameterization will be implemented.

Aspects of the model simulation thought to be critical for MJO simulation were analyzed using recently developed process-oriented diagnostics. LR E3SMv1 slightly underestimates moisture-convection coupling (Figure 16a),

particularly because the lower free-troposphere is not dry enough for the weak precipitation regimes (i.e., precipitation percentile <40). Given that models tend to simulate a stronger MJO with a tighter moisture-convection coupling, our results suggest the possibility to improve MJO simulation fidelity in the model by enhancing the convection sensitivity to moisture. The longwave cloud-radiation feedback was found to be underestimated for weak precipitation anomalies (Figure 16b). Examining clouds in the weakly perturbed columns is warranted to improve the longwave cloud-radiation feedback, the main maintenance process for the MJO in the model (Figure 5). It was found that the vertical profiles of the mean state vertical velocity and MSE over the Indo-Pacific warm pool were realistically represented in LR E3SMv1 (Figures 16c and 16d), despite the dry bias throughout the troposphere, yielding the NGMS metric that is close to the observed. The good performance in the mean state overturning circulation likely contributed to the decent performance of the model in capturing MJO variability.

Collectively, our results have demonstrated that E3SMv1 is an excellent community tool to study the MJO and its associated extreme events in the current and future climates. As a follow-up study, we have been analyzing the modulation of tropical cyclones by MJO in the HR E3SMv1 simulation, the results of which will be reported in a separate study.

Data Availability Statement

The E3SM project, code, simulation configurations, model output, and tools to work with the output are described at the website https://e3sm.org. Instructions on how to get started running E3SM are available at the website https://e3sm.org/model/running-e3sm/e3sm-quick-start. All model codes may be accessed on the GitHub repository (https://github.com/E3SM-Project/E3SM). Model output data are accessible directly on NERSC (https://portal.nersc.gov/archive/home/d/dkang/www/E3SM_data_JAMES). The sources for various observational data used in this study are as follows: TRMM precipitation (https://gpm.nasa.gov/data/directory), ERA5 reanalysis (https://www.ecmwf.int/en/forecasts/datasets/reanalysis-datasets/era5), NOAA daily interpolated OLR (https://psl.noaa.gov/data/gridded/data.interp_OLR.html), and HadISST (https://www.metoffice.gov.uk/hadobs/hadisst/).

Acknowledgments
D. Kim was supported by the DOE RGMA program (DE-SC0016223), the NOAA CVP program (NA18OAR4310300), the NASA MAP program (80NSSC17K0227), and the Brain Pool program funded by the Ministry of Science and ICT through the National Research Foundation of Korea (NRF-2021H1D3A2A01039352). D. Kang was supported by Sejong Science Fellowship funded by the National Research Foundation of Korea (NRF-2021R1C1C2004621). Work of the LLNL-affiliated author (M.-S. Ahn) was performed under the auspices of the U.S. Department of Energy by Lawrence Livermore National Laboratory under Contract DE-AC52-07NA27344 and their efforts were supported by the Regional and Global Model Analysis program area of the United States Department of Energy's Office of Science. C. DeMott and C.-W. Hsu were supported by the DOE RGMA program (DE-SC0020092). C. Yoo were supported by the National Research Foundation of Korea (NRF-2018R1A6A1A08025520 and NRF-2019R1C1C1003161). R. Leung, S. Hagos, and P. Rasch were also supported by the Office of Science of U.S. Department of Energy Biological and Environmental Research as part of the Regional and Global Model Analysis program area. PNNL is operated for the Department of Energy by Battelle Memorial Institute under contract DE-AC05-76RL01830.

References

Abatzoglou, J. T., & Brown, T. J. (2009). Influence of the Madden-Julian oscillation on summertime cloud-to-ground lightning activity over the continental United States. *Monthly Weather Review*, *137*, 3596–3601. https://doi.org/10.1175/2009MWR3019.1

Ahn, M.-S., Kim, D., Ham, Y.-G., & Park, S. (2020). Role of maritime continent land convection on the mean state and MJO propagation. *Journal of Climate*, *33*, 1659–1675. https://doi.org/10.1175/JCLI-D-19-0342.1

Ahn, M.-S., Kim, D., Kang, D., Lee, J., Sperber, K. R., Gleckler, P. J., et al. (2020). MJO propagation across the maritime continent: Are CMIP6 models better than CMIP5 models? *Geophysical Research Letters*, *47*, e2020GL087250. https://doi.org/10.1029/2020GL087250

Ahn, M.-S., Kim, D., Sperber, K. R., Kang, I.-S., Maloney, E., Waliser, D., et al. (2017). MJO simulation in CMIP5 climate models: MJO skill metrics and process-oriented diagnosis. *Climate Dynamics*, *49*, 1–4045. https://doi.org/10.1007/s00382-017-3558-4

Andersen, J. A., & Kuang, Z. (2012). Moist static energy budget of MJO-like disturbances in the atmosphere of a zonally symmetric aquaplanet. *Journal of Climate*, *25*, 2782–2804. https://doi.org/10.1175/JCLI-D-11-00168.1

Arnold, N. P., Kuang, Z., & Tziperman, E. (2013). Enhanced MJO-like variability at high SST. *Journal of Climate*, *26*, 988–1001. https://doi.org/10.1175/JCLI-D-12-00272.1

Balaguru, K., Leung, L. R., Van Roekel, L. P., Golaz, J. C., Ullrich, P. A., Caldwell, P. M., et al. (2020). Characterizing tropical cyclones in the energy Exascale Earth system model version 1. *Journal of Advances in Modeling Earth Systems*, *12*, 1–23. https://doi.org/10.1029/2019MS002024

Barnston, A. G., & Livezey, R. E. (1987). Classification, seasonality and persistence of low-frequency atmospheric circulation patterns. *Monthly Weather Review*, *115*, 1083–1126. https://doi.org/10.1175/1520-0493(1987)115<1083:CSAPOL>2.0.CO;2

Baranowski, D. B., Waliser, D. E., Jiang, X., Ridout, J. A., & Flatau, M. K. (2019). Contemporary GCM fidelity in representing the diurnal cycle of precipitation over the maritime continent. *Journal of Geophysical Research: Atmosphere*, *124*, 747–769. https://doi.org/10.1029/2018JD029474

Benedict, J. J., Maloney, E. D., Sobel, A. H., & Frierson, D. M. W. (2014). Gross moist stability and MJO simulation skill in three full-physics GCMs. *Journal of the Atmospheric Sciences*, *71*, 3327–3349. https://doi.org/10.1175/JAS-D-13-0240.1

Bond, N. A., & Vecchi, G. A. (2003). The influence of the Madden–Julian oscillation on precipitation in Oregon and Washington. *Weather and Forecasting*, *18*, 600–613. https://doi.org/10.1175/1520-0434(2003)018<0600:TIOTMO>2.0.CO;2

Bretherton, C. S., Peters, M. E., & Back, L. E. (2004). Relationships between water vapor path and precipitation over the tropical oceans. *Journal of Climate*, *17*, 1517–1528. https://doi.org/10.1175/1520-0442(2004)017<1517:RBWVPA>2.0.CO;2

Caldwell, P. M., Mametjanov, A., Tang, Q., Van Roekel, L. P., Golaz, J.-C., Lin, W., et al. (2019). The DOE E3SM coupled model version 1: Description and results at high resolution. *Journal of Advances in Modeling Earth Systems*, *11*, 4095–4146. https://doi.org/10.1029/2019MS001870

DeMott, C. A., Klingaman, N. P., Tseng, W. L., Burt, M. A., Gao, Y., Randall, D. A., & Randall, D. A. (2019). The convection connection: How ocean feedbacks affect tropical mean moisture and MJO propagation. *Journal of Geophysical Research: Atmosphere*, *124*, 11910–11931. https://doi.org/10.1029/2019JD031015

DeMott, C. A., Wolding, B. O., Maloney, E. D., Randall, D. A., & Randall, D. A. (2018). Atmospheric mechanisms for MJO decay over the maritime continent. *Journal of Geophysical Research: Atmosphere*, *123*, 5188–5204. https://doi.org/10.1029/2017JD026979

Feldstein, S. B. (2000). The timescale, power spectra, and climate noise properties of teleconnection patterns. *Journal of Climate*, *13*, 4430–4440. https://doi.org/10.1175/1520-0442(2000)013<4430:TTPSAC>2.0.CO;2

Feng, J., Li, T., & Zhu, W. (2015). Propagating and nonpropagating MJO events over maritime continent. *Journal of Climate*, *28*, 8430–8449. https://doi.org/10.1175/JCLI-D-15-0085.1

Golaz, J. C., Caldwell, P. M., Van Roekel, L. P., Petersen, M. R., Tang, Q., Wolfe, J. D., et al. (2019). The DOE E3SM coupled model version 1: Overview and evaluation at standard resolution. *Journal of Advances in Modeling Earth Systems*, *11*, 2089–2129. https://doi.org/10.1029/2018MS001603

Gonzalez, A. O., & Jiang, X. (2017). Winter mean lower tropospheric moisture over the Maritime Continent as a climate model diagnostic metric for the propagation of the Madden-Julian oscillation. *Geophysical Research Letters*, *44*, 2588–2596. https://doi.org/10.1002/2016GL072430

Gonzalez, A. O., & Jiang, X. (2019). Distinct propagation characteristics of intraseasonal variability over the tropical West Pacific. *Journal of Geophysical Research: Atmosphere*, *124*, 5332–5351. https://doi.org/10.1029/2018JD029884

Gushchina, D., & Dewitte, B. (2012). Intraseasonal tropical atmospheric variability associated with the two flavors of El Niño. *Monthly Weather Review*, *140*, 3669–3681. https://doi.org/10.1175/MWR-D-11-00267.1

Hagos, S., Leung, L. R., Garuba, O., & Patricola, C. M. (2021). Influence of background divergent moisture flux on the frequency of North Pacific atmospheric rivers. *Journal of Climate*, *34*, 6129–6133. https://doi.org/10.1175/jcli-d-21-0058.1

Hagos, S. M., Leung, L. R., Garuba, O. A., Demott, C., Harrop, B., Lu, J., & Ahn, M.-S. (2021). The relationship between precipitation and precipitable water in CMIP6 simulations and implications for tropical climatology and change. *Journal of Climate*, *34*, 1587–1600. https://doi.org/10.1175/JCLI-D-20-0211.1

Hagos, S. M., Zhang, C., Feng, Z., Burleyson, C. D., De Mott, C., Kerns, B., et al. (2016). The impact of the diurnal cycle on the propagation of Madden-Julian oscillation convection across the Maritime Continent. *Journal of Advances in Modeling Earth Systems*, *8*, 1552–1564. https://doi.org/10.1002/2016MS000725

Harrop, B. E., Ma, P. L., Rasch, P. J., Neale, R. B., & Hannay, C. (2018). The role of convective gustiness in reducing seasonal precipitation biases in the tropical West Pacific. *Journal of Advances in Modeling Earth Systems*, *10*, 961–970. https://doi.org/10.1002/2017MS001157

Henderson, S. A., Maloney, E. D., & Son, S.-W. (2017). Madden–Julian oscillation Pacific teleconnections: The impact of the basic state and MJO representation in general circulation models. *Journal of Climate*, *30*, 4567–4587. https://doi.org/10.1175/JCLI-D-16-0789.1

Hendon, H. H., & Abhik, S. (2018). Differences in vertical structure of the Madden-Julian oscillation associated with the quasi-biennial oscillation. *Geophysical Research Letters*, *45*, 4419–4428. https://doi.org/10.1029/2018GL077207

Hersbach, H., Bell, B., Berrisford, P., Hirahara, S., Horányi, A., Muñoz-Sabater, J., et al. (2020). The ERA5 global reanalysis. *Quarterly Journal of the Royal Meteorological Society*, *146*, 1999–2049. https://doi.org/10.1002/qj.3803

Hoskins, B. J., & Ambrizzi, T. (1993). Rossby wave propagation on a realistic longitudinally varying flow. *Journal of the Atmospheric Sciences*, *50*, 1661–1671. https://doi.org/10.1175/1520-0469(1993)050<1661:RWPOAR>2.0.CO;2

Hoskins, B. J., & Karoly, D. J. (1981). The steady linear response of a spherical atmosphere to thermal and orographic forcing. *Journal of the Atmospheric Sciences*, *38*, 1179–1196. https://doi.org/10.1175/1520-0469(1981)038<1179:TSLROA>2.0.CO;2

Huffman, G. J., Bolvin, D. T., Nelkin, E. J., Wolff, D. B., Adler, R. F., Gu, G., et al. (2007). The TRMM multisatellite precipitation analysis (TMPA): Quasi-global, multiyear, combined-sensor precipitation estimates at fine scales. *Journal of Hydrometeorology*, *8*, 38–55. https://doi.org/10.1175/JHM560.1

Inness, P. M., Slingo, J. M., Woolnough, S. J., Neale, R. B., & Pope, V. D. (2001). Organization of tropical convection in a GCM with varying vertical resolution; implications for the simulation of the Madden-Julian oscillation. *Climate Dynamics*, *17*, 777–793. https://doi.org/10.1007/s003820000148

Inoue, K., Adames, Á. F., & Yasunaga, K. (2020). Vertical velocity profiles in convectively coupled equatorial waves and MJO: New diagnoses of vertical velocity profiles in the wavenumber–frequency domain. *Journal of the Atmospheric Sciences*, *77*, 2139–2162. https://doi.org/10.1175/JAS-D-19-0209.1

Jeong, J.-H., Ho, C.-H., Kim, B.-M., & Kwon, W.-T. (2005). Influence of the Madden-Julian oscillation on wintertime surface air temperature and cold surges in East Asia. *Journal of Geophysical Research*, *110*, D11104. https://doi.org/10.1029/2004JD005408

Jiang, X. (2017). Key processes for the eastward propagation of the Madden-Julian Oscillation based on multimodel simulations. *Journal of Geophysical Research: Atmosphere*, *122*, 755–770. https://doi.org/10.1002/2016JD025955

Jiang, X., Adames, Á. F., Kim, D., Maloney, E. D., Lin, H., Kim, H., et al. (2020). Fifty years of research on the Madden-Julian oscillation: Recent progress, challenges, and perspectives. *Journal of Geophysical Research: Atmosphere*, *125*, e2019JD030911. https://doi.org/10.1029/2019JD030911

Jiang, X., Su, H., & Waliser, D. E. (2019). A damping effect of the maritime continent for the Madden-Julian oscillation. *Journal of Geophysical Research: Atmosphere*, *124*, 13693–13713. https://doi.org/10.1029/2019JD031503

Jiang, X., Waliser, D. E., Xavier, P. K., Petch, J., Klingaman, N. P., Woolnough, S. J., et al. (2015). Vertical structure and physical processes of the Madden-Julian oscillation: Exploring key model physics in climate simulations. *Journal of Geophysical Research: Atmosphere*, *120*, 4718–4748. https://doi.org/10.1002/2014JD022375

Jones, C., & Carvalho, L. M. V. (2012). Spatial-intensity variations in extreme precipitation in the contiguous United States and the Madden-Julian oscillation. *Journal of Climate*, *25*, 4898–4913. https://doi.org/10.1175/JCLI-D-11-00278.1

Kang, D., Kim, D., Ahn, M.-S., & An, S.-I. (2021). The role of background meridional moisture gradient on the propagation of the MJO over the maritime continent. *Journal of Climate*, 1–54. https://doi.org/10.1175/JCLI-D-20-0085.1

Kang, D., Kim, D., Ahn, M.-S., Neale, R., Lee, J., & Gleckler, P. J. (2020). The role of the mean state on MJO simulation in CESM2 ensemble simulation. *Geophysical Research Letters*, *47*, e2020GL089824. https://doi.org/10.1029/2020GL089824

Kerns, B. W., & Chen, S. S. (2020). A 20-year climatology of Madden-Julian oscillation convection: Large-scale precipitation tracking from TRMM-GPM rainfall. *Journal of Geophysical Research: Atmosphere*, *125*, 1–21. https://doi.org/10.1029/2019JD032142

Kim, D., Ahn, M.-S., Kang, I.-S., & Del Genio, A. D. (2015). Role of longwave cloud–radiation feedback in the simulation of the Madden–Julian oscillation. *Journal of Climate*, *28*, 6979–6994. https://doi.org/10.1175/JCLI-D-14-00767.1

Kim, D., Kim, H., & Lee, M.-I. (2017). Why does the MJO detour the Maritime Continent during austral summer? *Geophysical Research Letters*, *44*, 2579–2587. https://doi.org/10.1002/2017GL072643

Kim, D., Kug, J.-S., & Sobel, A. H. (2014). Propagating versus nonpropagating Madden–Julian oscillation events. *Journal of Climate*, *27*, 111–125. https://doi.org/10.1175/JCLI-D-13-00084.1

Kim, D., & Maloney, E. D. (2017). Simulation of the Madden-Julian oscillation using general circulation models. In C. P. Chang, et al. (Eds.), *The global monsoon system* (3rd ed., pp. 119–130). https://doi.org/10.1142/9789813200913_0009

Kim, D., Maloney, E. D., Zhang, C., Kim, D., Lau, G. N. C., & Wang, B. (2021). Review: MJO propagation over the maritime continent, Chap. 21. In C. P. Chang, K. J. Ha, R. H. Johnson, D. Kim, G. N. Lau, & B. Wang (Eds.), *The multiscale global monsoon system. World scientific series on Asia-Pacific weather and climate* (Vol. 11). World Scientific. https://doi.org/10.1142/11723

Kim, D., Sobel, A. H., Del Genio, A. D., Chen, Y., Camargo, S. J., Yao, M.-S., et al. (2012). The tropical subseasonal variability simulated in the NASA GISS general circulation model. *Journal of Climate*, *25*, 4641–4659. https://doi.org/10.1175/JCLI-D-11-00447.1

Kim, D., Sobel, A. H., Maloney, E. D., Frierson, D. M. W., & Kang, I.-S. (2011). A systematic relationship between intraseasonal variability and mean state bias in AGCM simulations. *Journal of Climate*, *24*, 5506–5520. https://doi.org/10.1175/2011jcli4177.1

Kim, D., Xavier, P., Maloney, E., Wheeler, M., Waliser, D., Sperber, K., et al. (2014). Process-oriented MJO simulation diagnostic: Moisture sensitivity of simulated convection. *Journal of Climate*, *27*, 5379–5395. https://doi.org/10.1175/JCLI-D-13-00497.1

Kim, H., Caron, J. M., Richter, J. H., & Simpson, I. R. (2020). The lack of QBO-MJO connection in CMIP6 models. *Geophysical Research Letters*, *47*, 1–8. https://doi.org/10.1029/2020GL087295

Kiranmayi, L., & Maloney, E. D. (2011). Intraseasonal moist static energy budget in reanalysis data. *Journal of Geophysical Research*, *116*, D21117. https://doi.org/10.1029/2011JD016031

Klingaman, N. P., & Demott, C. A. (2020). Mean state biases and interannual variability affect perceived sensitivities of the Madden-Julian oscillation to air-sea coupling. *Journal of Advances in Modeling Earth Systems*, *12*, 1–22. https://doi.org/10.1029/2019MS001799

Klotzbach, P., Abhik, S., Hendon, H. H., Bell, M., Lucas, C., Marshall, A. G., & Oliver, E. C. J. (2019). On the emerging relationship between the stratospheric Quasi-Biennial oscillation and the Madden-Julian oscillation. *Scientific Reports*, *9*, 1–9. https://doi.org/10.1038/s41598-019-40034-6

Klotzbach, P. J. (2014). The Madden–Julian oscillation's impacts on worldwide tropical cyclone activity. *Journal of Climate*, *27*, 2317–2330. https://doi.org/10.1175/JCLI-D-13-00483.1

Lee, J. C. K., & Klingaman, N. P. (2018). The effect of the quasi-biennial oscillation on the Madden–Julian oscillation in the Met Office unified model global ocean mixed layer configuration. *Atmospheric Science Letters*, *19*, 1–10. https://doi.org/10.1002/asl.816

Leung, L. R., Bader, D. C., Taylor, M. A., & McCoy, R. B. (2020). An introduction to the E3SM special collection: Goals, science drivers, development, and analysis. *Journal of Advances in Modeling Earth Systems*, *12*, e2019MS001821. https://doi.org/10.1029/2019MS001821

Liebmann, C. A., & Smith, B. (1996). Description of a complete (interpolated) outgoing longwave radiation dataset. *Bulletin of the American Meteorological Society*, *77*, 1275–1277.

Lin, J. L., & Mapes, B. E. (2004). Radiation budget of the tropical intraseasonal oscillation. *Journal of the Atmospheric Sciences*, *61*, 2050–2062. https://doi.org/10.1175/1520-0469(2004)061<2050:RBOTTI>2.0.CO;2

Ling, J., Zhang, C., Wang, S., & Li, C. (2017). A new interpretation of the ability of global models to simulate the MJO. *Geophysical Research Letters*, *44*, 5798–5806. https://doi.org/10.1002/2017GL073891

Madden, R. A., & Julian, P. R. (1971). Detection of a 40–50 day oscillation in the zonal wind in the tropical Pacific. *Journal of the Atmospheric Sciences*, *28*, 702–708. https://doi.org/10.1175/1520-0469(1971)028<0702:DOADOI>2.0.CO;2

Madden, R. A., & Julian, P. R. (1972). Description of global-scale circulation cells in the tropics with a 40–50 day period. *Journal of the Atmospheric Sciences*, *29*, 1109–1123. https://doi.org/10.1175/1520-0469(1972)029<1109:DOGSCC>2.0.CO;2

Maloney, E. D. (2009). The moist static energy budget of a composite tropical intraseasonal oscillation in a climate model. *Journal of Climate*, *22*, 711–729. https://doi.org/10.1175/2008JCLI2542.1

Mapes, B., & Neale, R. (2011). Parameterizing convective organization to escape the entrainment dilemma. *Journal of Advances in Modeling Earth Systems*, *3*, M06004. https://doi.org/10.1029/2011ms000042

Martin, Z., Orbe, C., Wang, S., & Sobel, A. (2021a). The MJO-QBO relationship in a GCM with stratospheric nudging. *Journal of Climate*, 1–69. https://doi.org/10.1175/JCLI-D-20-0636.1

Martin, Z., Son, S.-W., Butler, A., Hendon, H., Kim, H., Sobel, A., et al. (2021b). The influence of the quasi-biennial oscillation on the Madden–Julian oscillation. *Nature Reviews Earth & Environment*, *2*, 477–489. https://doi.org/10.1038/s43017-021-00173-9

Mori, M., & Watanabe, M. (2008). The growth and triggering mechanisms of the PNA: A MJO-PNA coherence. *Journal of the Meteorological Society of Japan. Series II*, *86*, 213–236. https://doi.org/10.2151/jmsj.86.213

Neelin, J. D., & Held, I. M. (1987). Modeling tropical convergence based on the moist static energy budget. *Monthly Weather Review*, *115*, 3–12. https://doi.org/10.1175/1520-0493(1987)115<0003:MTCBOT>2.0.CO;2

Nishimoto, E., & Yoden, S. (2017). Influence of the stratospheric quasi-biennial oscillation on the Madden–Julian oscillation during Austral summer. *Journal of the Atmospheric Sciences*, *74*, 1105–1125. https://doi.org/10.1175/JAS-D-16-0205.1

Orbe, C., Roekel, L. V., Adames, Á. F., Dezfuli, A., Fasullo, J., Gleckler, P. J., et al. (2020). Representation of modes of variability in six U.S. climate models. *Journal of Climate*, *33*, 7591–7617. https://doi.org/10.1175/jcli-d-19-0956.1

Peatman, S. C., Matthews, A. J., & Stevens, D. P. (2014). Propagation of the Madden–Julian oscillation through the maritime continent and scale interaction with the diurnal cycle of precipitation. *Quarterly Journal of the Royal Meteorological Society*, *140*, 814–825. https://doi.org/10.1002/qj.2161

Peters, O., & Neelin, J. (2006). Critical phenomena in atmospheric precipitation. *Nature Physics*, *2*, 393–396. https://doi.org/10.1038/nphys314

Pohl, B., & Matthews, A. J. (2007). Observed changes in the lifetime and amplitude of the Madden–Julian oscillation associated with interannual ENSO sea surface temperature anomalies. *Journal of Climate*, *20*, 2659–2674. https://doi.org/10.1175/JCLI4230.1

Rasch, P. J., Xie, S., Ma, P. L., Lin, W., Wang, H., Tang, Q., et al. (2019). An overview of the atmospheric component of the energy exascale Earth system model. *Journal of Advances in Modeling Earth Systems*, *11*, 2377–2411. https://doi.org/10.1029/2019MS001629

Raymond, D. J., Sessions, S. L., Sobel, A. H., & Fuchs, Ž. (2009). The mechanics of gross moist stability. *Journal of Advances in Modeling Earth Systems*, *1*, 9. https://doi.org/10.3894/JAMES.2009.1.9

Rayner, N. A., Parker, D. E., Horton, E. B., Folland, C. K., Alexander, L. V., Rowell, D. P., et al. (2003). Global analyses of sea surface temperature, sea ice, and night marine air temperature since the late nineteenth century. *Journal of Geophysical Research*, *108*, 4407. https://doi.org/10.1029/2002JD002670

Reid, J. S., Xian, P., Hyer, E. J., Flatau, M. K., Ramirez, E. M., Turk, F. J., et al. (2012). Multi-scale meteorological conceptual analysis of observed active fire hotspot activity and smoke optical depth in the Maritime Continent. *Atmospheric Chemistry and Physics*, *12*, 2117–2147. https://doi.org/10.5194/acp-12-2117-2012

Ren, P., Kim, D., Ahn, M.-S., Kang, D., & Ren, H.-L. (2021). Intercomparison of MJO column moist static energy and water vapor budget among six modern reanalysis products. *Journal of Climate*, *34*, 2977–3001. https://doi.org/10.1175/JCLI-D-20-0653.1

Richter, J. H., Chen, C. C., Tang, Q., Xie, S., & Rasch, P. J. (2019). Improved simulation of the QBO in E3SMv1. *Journal of Advances in Modeling Earth Systems*, *11*, 3403–3418. https://doi.org/10.1029/2019MS001763

Rushley, S. S., Kim, D., Bretherton, C. S., & Ahn, M.-S. (2018). Reexamining the nonlinear moisture-precipitation relationship over the tropical oceans. *Geophysical Research Letters*, *45*, 1133–1140. https://doi.org/10.1002/2017GL076296

Sakaeda, N., Dias, J., & Kiladis, G. N. (2020). The unique characteristics and potential mechanisms of the MJO-QBO relationship. *Journal of Geophysical Research: Atmospheres*, *125*, e2020JD033196. https://doi.org/10.1029/2020JD033196

Sardeshmukh, P. D., & Hoskins, B. J. (1988). The generation of global rotational flow by steady idealized tropical divergence. *Journal of the Atmospheric Sciences*, *45*, 1228–1251. https://doi.org/10.1175/1520-0469(1988)045<1228:TGOGRF>2.0.CO;2

Slingo, J. M., Rowell, D. P., Sperber, K. R., & Nortley, F. (1999). On the predictability of the interannual behaviour of the Madden-Julian oscillation and its relationship with El Niño. *Quarterly Journal of the Royal Meteorological Society*, *125*, 583–609. https://doi.org/10.1002/qj.49712555411

Sobel, A., Wang, S., & Kim, D. (2014). Moist static energy budget of the MJO during DYNAMO. *Journal of the Atmospheric Sciences*, *71*, 4276–4291. https://doi.org/10.1175/JAS-D-14-0052.1

Sobel, A. H., Maloney, E. D., Bellon, G., & Frierson, D. M. (2008). The role of surface heat fluxes in tropical intraseasonal oscillations. *Nature Geoscience*, *1*, 653–657. https://doi.org/10.1038/ngeo312

Sobel, A. H., Maloney, E. D., Bellon, G., & Frierson, D. M. (2010). Surface fluxes and tropical intraseasonal variability: A reassessment. *Journal of Advances in Modeling Earth Systems*, *2*, 2. https://doi.org/10.3894/JAMES.2010.2.2

Son, S.-W., Lim, Y., Yoo, C., Hendon, H. H., & Kim, J. (2017). Stratospheric control of the Madden–Julian oscillation. *Journal of Climate*, *30*, 1909–1922. https://doi.org/10.1175/JCLI-D-16-0620.1

Stan, C., & Straus, D. M. (2019). The impact of cloud representation on the sub-seasonal forecasts of atmospheric teleconnections and preferred circulation regimes in the northern hemisphere. *Atmosphere-Ocean*, *57*, 233–248. https://doi.org/10.1080/07055900.2019.1590178

Stan, C., Straus, D. M., Frederiksen, J. S., Lin, H., Maloney, E. D., & Schumacher, C. (2017). Review of tropical-extratropical teleconnections on intraseasonal time scales. *Reviews of Geophysics*, *55*, 902–937. https://doi.org/10.1002/2016RG000538

Tam, C.-Y., & Lau, N.-C. (2005). Modulation of the Madden-Julian oscillation by ENSO: Inferences from observations and GCM simulations. *Journal of the Meteorological Society of Japan. Series II*, *83*, 727–743. https://doi.org/10.2151/jmsj.83.727

Tang, S., Gleckler, P., Xie, S., Lee, J., Ahn, M.-S., Covey, C., & Zhang, C. (2021). Evaluating diurnal and semi-diurnal cycle of precipitation in CMIP6 models using satellite- and ground-based observations. *Journal of Climate*, 1–56. https://doi.org/10.1175/JCLI-D-20-0639.1

Thompson, D. B., & Roundy, P. E. (2013). The relationship between the Madden-Julian oscillation and U.S. violent tornado outbreaks in the spring. *Monthly Weather Review*, *141*, 2087–2095. https://doi.org/10.1175/MWR-D-12-00173.1

Tseng, K.-C., Maloney, E., & Barnes, E. (2019). The consistency of MJO teleconnection patterns: An explanation using linear Rossby wave theory. *Journal of Climate*, *32*, 531–548. https://doi.org/10.1175/JCLI-D-18-0211.1

Wang, B., & Rui, H. (1990). Synoptic climatology of transient tropical intraseasonal convection anomalies: 1975–1985. *Meteorology and Atmospheric Physics*, *44*, 43–61. https://doi.org/10.1007/BF01026810

Wang, J., Kim, H., Kim, D., Henderson, S. A., Stan, C., & Maloney, E. D. (2020a). MJO teleconnections over the PNA region in climate models. Part I: Performance- and process-based skill metrics. *Journal of Climate*, *33*, 1051–1067. https://doi.org/10.1175/JCLI-D-19-0253.1

Wang, J., Kim, H., Kim, D., Henderson, S. A., Stan, C., & Maloney, E. D. (2020b). MJO teleconnections over the PNA region in climate models. Part II: Impacts of the MJO and basic state. *Journal of Climate*, *33*, 5081–5101. https://doi.org/10.1175/JCLI-D-19-0865.1

Wei, Y., & Ren, H. L. (2019). Modulation of ENSO on fast and slow MJO modes during boreal winter. *Journal of Climate*, *32*, 7483–7506. https://doi.org/10.1175/JCLI-D-19-0013.1

Weickmann, K. M. (1983). Intraseasonal circulation and outgoing longwave radiation modes during northern hemisphere winter. *Monthly Weather Review*, *111*, 1838–1858. https://doi.org/10.1175/1520-0493(1983)111<1838:ICAOLR>2.0.CO;2

Wheeler, M. C., & Hendon, H. H. (2004). An all-season real-time multivariate MJO index: Development of an index for monitoring and prediction. *Monthly Weather Review*, *132*, 1917–1932. https://doi.org/10.1175/1520-0493(2004)132<1917:AARMMI>2.0.CO;2

Wolding, B. O., Maloney, E. D., & Branson, M. (2016). Vertically resolved weak temperature gradient analysis of the Madden-Julian oscillation in SP-CESM. *Journal of Advances in Modeling Earth Systems*, *8*, 1586–1619. https://doi.org/10.1002/2016MS000724

Woolnough, S. J., Slingo, J. M., & Hoskins, B. J. (2000). The relationship between convection and Sea surface temperature on intraseasonal timescales. *Journal of Climate*, *13*, 2086–2104. https://doi.org/10.1175/1520-0442(2000)013<2086:TRBCAS>2.0.CO;2

Wu, C.-H., & Hsu, H.-H. (2009). Topographic influence on the MJO in the maritime continent. *Journal of Climate*, *22*, 5433–5448. https://doi.org/10.1175/2009JCLI2825.1

Xie, S., Lin, W., Rasch, P. J., Ma, P. L., Neale, R., Larson, V. E., et al. (2018). Understanding cloud and convective characteristics in version 1 of the E3SM atmosphere model. *Journal of Advances in Modeling Earth Systems*, *10*, 2618–2644. https://doi.org/10.1029/2018MS001350

Xie, S., Wang, Y. C., Lin, W., Ma, H. Y., Tang, Q., Tang, S., et al. (2019). Improved diurnal cycle of precipitation in E3SM with a revised convective triggering function. *Journal of Advances in Modeling Earth Systems*, *11*, 2290–2310. https://doi.org/10.1029/2019MS001702

Yoo, C., Park, S., Kim, D., Yoon, J.-H., & Kim, H.-M. (2015). Boreal winter MJO teleconnection in the community atmosphere model version 5 with the unified convection parameterization. *Journal of Climate*, *28*, 8135–8150. https://doi.org/10.1175/JCLI-D-15-0022.1

Yoo, C., & Son, S.-W. (2016). Modulation of the boreal wintertime Madden-Julian oscillation by the stratospheric quasi-biennial oscillation. *Geophysical Research Letters*, *43*, 1392–1398. https://doi.org/10.1002/2016GL067762

Zhang, C. (2013). Madden–Julian oscillation: Bridging weather and climate. *Bulletin of the American Meteorological Society*, *94*, 1849–1870. https://doi.org/10.1175/BAMS-D-12-00026.1

Zhang, C., & Ling, J. (2017). Barrier effect of the Indo-Pacific maritime continent on the MJO: Perspectives from tracking MJO precipitation. *Journal of Climate*, *30*, 3439–3459. https://doi.org/10.1175/JCLI-D-16-0614.1

Zhang, C., & Zhang, B. (2018). QBO-MJO connection. *Journal of Geophysical Research: Atmosphere*, *123*, 2957–2967. https://doi.org/10.1002/2017JD028171

Zhang, L., & Han, W. (2020). Barrier for the eastward propagation of Madden-Julian oscillation over the maritime continent: A possible new mechanism. *Geophysical Research Letters*, *47*, 1–12. https://doi.org/10.1029/2020GL090211

Zhou, Y., Kim, H., & Waliser, D. E. (2021). Atmospheric river lifecycle responses to the Madden-Julian oscillation. *Geophysical Research Letters*, *48*, e2020GL090983. https://doi.org/10.1029/2020GL090983